CHEMOELASTOPLASTIC ANALYSIS OF A COPPER-GRADED SILICON NANOROD FOR LITHIUM-ION BATTERY ANODE APPLICATION

by

CHAO JI

Presented to the Faculty of the Graduate School of

The University of Texas at Arlington in Partial Fulfillment

of the Requirements

for the Degree of

MASTER OF SCIENCE IN MECHANICAL ENGINEERING

THE UNIVERSITY OF TEXAS AT ARLINGTON

May 2013

To my dear father and mother for

their help and support throughout my life

ACKNOWLEDGEMENTS

I would first like to thank Dr. Bo Yang, who I deeply admired, to give me this opportunity to do the research on this project. With his patience and faith in my abilities help me to complete this thesis. Also, his constant guidance and encouragement make me go throughout both my undergraduate and graduate programs.

I am also grateful to Dr. Hao Jiang and Dr. Juraj Irsa for their patient guidance and help with their professional knowledge in the duration of this thesis. Then I would like to thank Dr. Wen S. Chan and Dr. Bo P. Wang for serve on my thesis committee. I have benefited a great deal from their graduate lectures. Finally, I would like to thank my parents and all my friends for all their supports and encouragements through these years.

March 20, 2013

ABSTRACT

CHEMOELASTOPLASTIC ANALYSIS OF A COPPER-GRADED SILICON NANOROD FOR LITHIUM-ION BATTERY ANODE APPLICATION

Chao Ji, M.S

The University of Texas at Arlington, 2012

Supervising Professor: Bo Yang

Lithium-ion batteries are currently widely used in electronics, electrical vehicles and other devices/machines. Along with the mounting demand for much improved performance in these developing technological fields, silicon was recognized to possess much higher energy capacity when used as an anode than graphite that is currently used. However, there occurs colossal volume expansion of silicon anode during the lithiation process. The material consequently suffers enormous stresses, especially, at the interface with a current collector, which deteriorate the device quickly during cycling. To prevent the active material (Si) from falling off from a current collector, nanoengineering strategies have been suggested, including nanostructuring and composition grading.

In the present thesis, we carry out a chemoelastoplastic analysis of a copper-graded silicon nanorod. From the end in contact with a current collector (taken to be copper), the nanorod composition starts with 100 % copper but is graded with decreasing copper content and increasing silicon content until a certain length in a grading zone. Beyond the grading zone, the composition is pure silicon. The deformation and stress due to steady-state insertion of lithium ions are examined by applying a finite element method. The effects of plasticity, finite

strain and finite rotation are taken into account, which are significant in this system with volume expansion of ~ 400 %. The results show that the grading zone can mitigate the stresses both in the rod and at the interface with a current collector. Rods with longer length of a grading zone enjoy lower stresses. This study in part lays out a base for designing graded silicon nanorods for improved performance in lithium-ion battery application.

TABLE OF CONTENTS

LIST OF ILLUSTRATIONS

Figure Page

LIST OF TABLES

CHAPTER 1

INTRODUCTION

1.1 Lithium-ion Battery Overview

Lithium-ion Batteries are currently wildly used in various electronic devices, and hybrid and electrical vehicles. The earlier development for Lithium-ion Battery can be traced back to 1960's. In metallic elements, lithium owns the properties with small density, large electronegativity, and possesses high energy density. However, the safety issues obstruct its commercialized because it's extremely flammable. In 1970's, Panasonic developed Li/(CFx)n battery which solved the safety problem. Meanwhile, Sanyo's Li/MnO2 battery was commonly used in calculators. But these batteries are primary batteries which are one time use only. The rechargeable, secondary Li-ion batteries we are using today were first invented by the Japanese company, SONY, in the early 90's. This battery employed carbon based anode which was the first time to use in the Li-ion battery. It has marked improvement on both safety and recharging cycles.

Compared with other types of rechargeable batteries such as Ni-Cd, Ni-Mh and Sealed batteries, Li-ion battery has the advantages as follow:

1. High energy density: 30%-40% lighter than Ni-Mh battery, and the capacity is 60% more in the same volume
2. Stable output voltage
3. No battery memory effect
4. Low self-discharge
5. Eco-friendly: not contain toxic elements such as Hg, Cd, Pb

On the other hand, the safety issue, although improved from predecessors, remains a problem. The chance of short circuit and explosion are much higher than other batteries. Several accidents about Li-ion batteries are reported every year.

1.2 Working Principle and Battery Anode

Today's Lithium-ion battery is made up of four main parts: cathode (positive electrode), anode (negative electrode), electrolyte and separator which are showed in Figure1.1

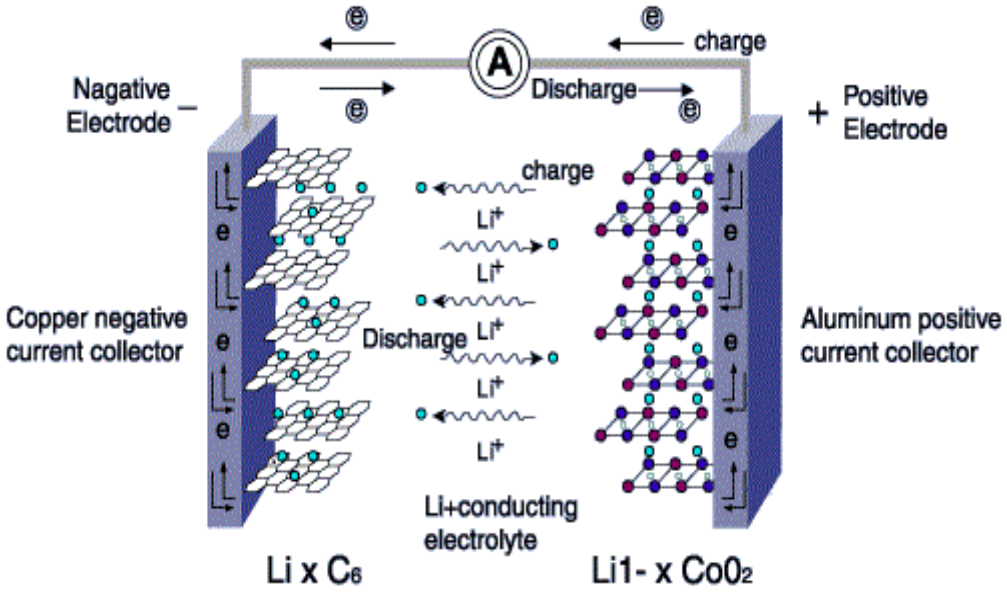

Figure 1.1 Battery inside structure [1]

All the lithium ion batteries work in almost the same way. Fig.1.2 shows that during the charging process, Lithium ions leave the cathode to anode through the electrolyte and insert into the anode structure. This process make the battery store the energy. When discharging occurs, the lithium ions are released by the anode and move back to cathode. Meanwhile, electrons flow through an outer circuit in order to maintain electroneutrality. The separator inside the battery makes the cathode and anode apart from each other. In both of the charging and discharging processes, lithium ions only move between the cathode and the anode, and the

electrons flow outside the electrodes. Such repetitive movement of lithium ions or so called charging and discharging is named as “rocking chair”

Specifically, chemical reactions within a graphite based lithium-ion battery are:

Cathode: $CoO_2+Li^++e^-=LiCoO_2$

Anode: $LiC_6-e^-=6C+Li^+$

Overall Reaction: $CoO_2+LiC_6=LiCoO_2+6C$

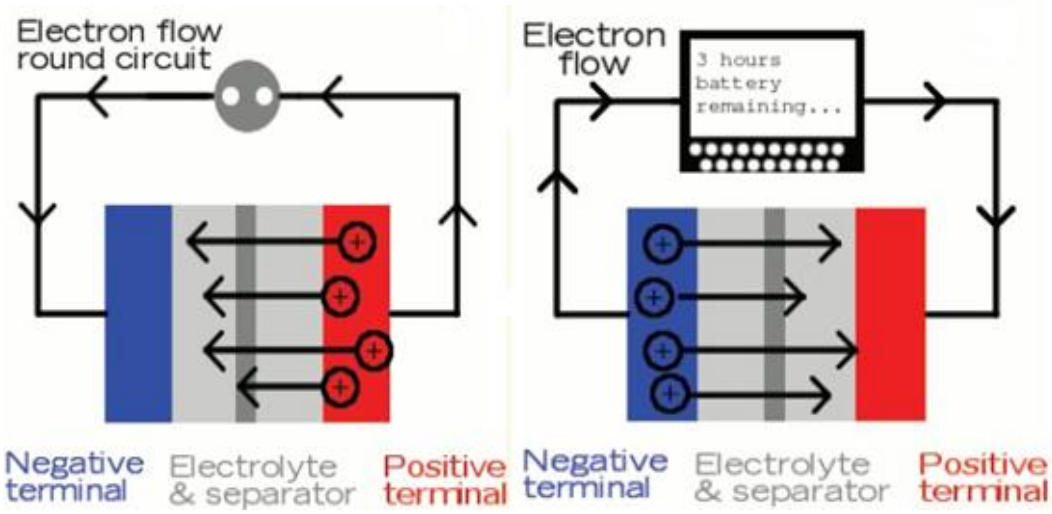

(a) (b)

Figure 1.2 Charging process [2]. (a) Charging process (b) Discharging process

Graphite based anode is the most commonly used right now. The anode structure is composed by stacking the carbon layers. The charging process is actually a process that lithium ions repeat intercalating to the carbon layers. Modifying battery anode is a way to improve the performances of Li-ion battery.

1.3 Ways of Modifying Anodes

1.3.1 Materials

In early development, simple substance of lithium was used as anode material but it is very dangerous because of its active material property. In charging process, pure lithium anode becomes crystalline and damage the separator which causes short circuit, electric leakage and

explosion. The crystalline problem is solved by using lithium alloy materials, for example, LiAl. However, new materials also bring new problems. The lithium alloy layers are not stable enough. After charging and discharging for several cycles, the anode structure would swell and pulverize, which lead to substantial capacity loss and rendering the battery dead.

So the performance of rechargeable battery is largely determined by what an anode material is used. Good anode materials should have the follwoing properties:

1. High material strength in chemo mechanical process
2. High reliability under cyclic lithiation and unlithiation
3. High lithium ion capacity
4. High Li-ion diffusion rate to improve the electrical conductivity
5. Low price and easy production

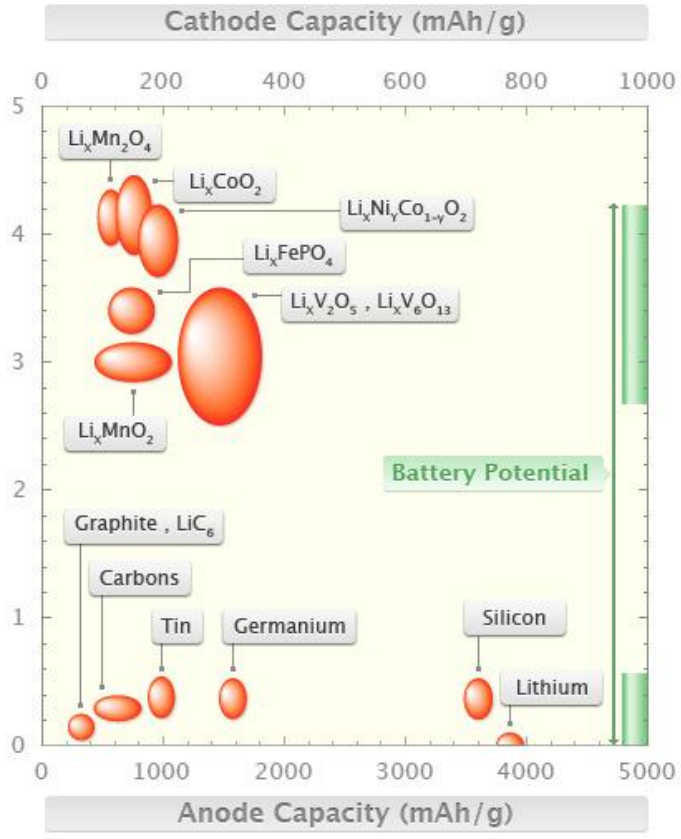

Figure 1.3 Electronic capacities of different materials [3]

Some anode materials which are into use or under research are introduced below.

1.3.1.1 Graphite:

Lithium ion can intercalate into graphite layered structure much easily in comparison to other early anode materials such as Li/MnO2. The intercalated graphite can remain stable. Carbon atoms arrange in hexagonal close-packed lattice, as showed in Fig.1.4. Theoretically, six carbon atoms can host one Li ion at most, which sets the capacity limit at 372mAh/g [4].

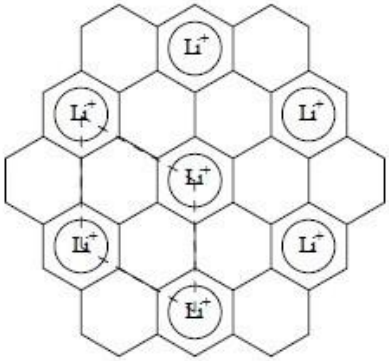

Figure 1.4 Molecular structure of LiC_6

The morphological change of graphite anode is about 10% after being fully charged. This means that the anode structure bears relatively low induced stresses rendering the batteries with high reliability and long usage life. At present, the retention rate of graphite anodes reaches > 90%. In addition, graphite is very low cost and easy to fabricate in present technology. Owing to the above advantageous properties, graphite base anode lithium-ion battery has been the most widely used so far for small electronics.

1.3.1.2 Tin (Sn):

Group IV elements, Si, Ge, and Sn, all have high capacity to store lithium ions, which can be the ideal candidates for the next generation lithium-ion battery.

Table 1.1 Properties of different anode materials [5]

Materials	Li	C	$Li_4Ti_5O_{12}$	Si	Sn	Sb	Al	Mg	Bi
Density/($g.cm^{-3}$)	0.53	2.25	3.5	2.33	7.29	6.7	2.7	1.3	9.78
Lithiated phase	Li	LiC_6	$Li_7Ti_5O_{12}$	$Li_{4.4}Si$	$Li_{4.4}Sn$	Li_3Sb	LiAl	Li_3Mg	Li_3Bi
Theoretical specific capacity/($mAh.g^{-1}$)	3862	372	175	4200	994	660	993	3350	385
Theoretical charge density/($mAh.cm^{-3}$)	2047	837	613	9786	7246	4422	268	4355	3765
Volume change/(%)	100	12	1	320	260	200	1	100	215
Potential vs. Li/(~V)	0	0.05	1.6	0.4	0.6	0.9	96 0.3	0.1	0.8

From Tab1.1, it can be seen that the theoretical specific capacity of Sn is 994mAh/g which is around 2.7 times higher than graphite. But before launching into application, some vital problems need to be solved first. The biggest problem is that during charging/discharging processes, it expands by 100-300% of its original volume. This enormous volume expansion induces huge stresses which cause cracking and pulverization to make capacity fading and anode failure. Another problem is that the melting point of pure Sn is relatively low (232℃). It's difficult to apply into mass production because of the complicated manufacturing techniques. Additionally, the prices of tin ores are not cheap and still keep increasing. So the cost the production cannot be controlled in a relatively low price rage.

1.3.1.3 Silicon (Si):

Silicon is known as the material with the highest theoretical specific capacity in group IV elements so far. Because of its special material property and atomic structure, each silicon atom can hold 4.4 lithium ions when it is fully charged. The capacity can reach up to about 4200 mAh/g, which is more than four times than Sn and ten times than the current commercial graphite based Li-ion anodes. This tremendous capacity difference has made silicon the most popular research subject for anode material application recently.

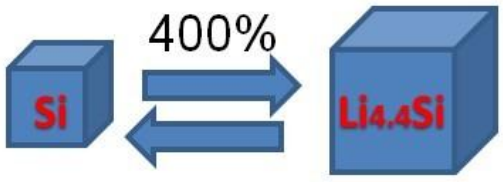

Figure 1.5 Volume expansion of LiSi compound

Besides, silicon is the second most abundant element on the earth. Furthermore, the fabrication technology of silicon is mature. Thus, the cost of silicon based lithium-ion battery is expected to be relatively low in the future.

However, silicon based anodes have a critical defect. Similar to Sn materials, the morphological change can reach up to 400% during the lithiation/delithiation, as schematically shown in Fig.1.5. In the meantime, the modulus varies by more than ten times. This tremendous volume change would cause damage to the electrode. For instance, the silicon anode may detatch from a current collector leading to battery failure with a short life.

1.3.1.4 Composite and alloy materials:

Using silicon composite and alloy materials may be a solution to the adverse effect of the huge volume change during lithiation and delithiation. The reason is that the mixing of other materials with silicon may still achieve higher capacity but can mitigate the deformation/stress consequence. For example, carbon based material has good rechargeable reliability according to the property of small deformation in lithiation process. Dimov, Kugino and Yoshio [6] presented a method of thermal vapor deposition (TVD). Silicon and graphite particles were milled into around 1-2 μm and mixed by ratio 1:1. Then benzene and toluene vapors were used as reactants to form the carbon-coated layer on the surface of silicon particles which can keep silicon particle from breaking up. The experimental results showed that this kind of material can be cycled at high current density and improve the uniformity of the lithiation. Hwang, lee, kong [7] developed electrospun core-shell fiber electrodes. In the core-shell fibers, nanoparticles in the core are wrapped by the carbon shell. This structure can resolve the issues of Si anode

operations, such as pulverization, losing contacts between Si and graphite conductors. It also shows relatively good electrical performance among silicon composite.

In comparison with carbon composites, metal alloys have been explored to enhance electronic conductivity and improve lithium insertion capacity. It has been experimented that coating of ductile metal particles like Fe, Co and Cu on Si can significantly improves the electrical contact and cyclability within charge and discharge [4]. In the present thesis, CuSi alloy is examined for lithium ion anode application. Copper element is known to own the second highest electrical conductivity in all elements, only lower than silver. But the cost is much cheaper than silver. On the other hand, copper does not react with lithium ions and hence can reduce the overall expansion of silicon mixed with copper during lithiation. Thus, the combination of copper and silicon is believed to increase the cycling efficiency and the rate capability. In recent research, Sethuraman, kowolik and Srinivasan [8] found that copper appears to act as glue that binds the electrode together and prevents the electronic isolation of silicon particles, consequently decreasing capacity loss. Murugesan, Harris, Lorgel and Stevenson [4] presented an approach for synthesizing copper coated amorphous Si particles through a polyol reduction method. The experimental results demonstrated that copper coating of Si can (1) reduce charge transfer resistance, (2) be highly reversible and increase charge storage capacity, (3) improve tolerance to volume expansion.

1.3.2 Size and Shape of Si Based Anode

In order to reduce the intensive stresses induced by volume expansion, nano engineering approaches have been studied. It raises intriguing questions to the nanoscale fracture and deformation mechanisms. That could be different from those macroscopic ones. It has been proved that many materials at the nanoscale are more ductile than they are at the normal sizes. For example, silicon is brittle in bulk sate and easy to fracture, but its strength can reach to the material theoretical value when it is in the nanometer size [9]. Nano-silicon based anode may have greater strength/toughness. The small size also means shorter diffusion length

and hence can reduce the stress magnitude for the same lithiation/delithiation rate. Several silicon nanostructures have been tested so far, including thin films, nano particles and nanowires.

1.3.2.1 Thin-film Anode

Silicon materials are brittle in bulk state. They have poor cyclic performance because they are easy to fracture [9]. So thin film structure was brought to our view. The experiments show the evidences that silicon thin films have better performance on capacity fading than bulk silicon [10]. Thin films can efficiently decrease the size effect on vertical direction that release the stress induced by size expansion. It is also showed that the thinner the film thickness is, the better cycleability it has [11]. Guo, Zhao and Yin [8] made the silicon thin films with the thickness from 100-530 nm by radio frequency magnetron sputtering. The experiment show that the 312 nm Si film has the highest reversible specific capacity over 3500 mAh/g and up to 90% capacity left (3150 mAh/g) after 25 charging cycles with 0.5C charge/discharge rate. Meanwhile, the 512nm film has fast capacity fading with the incensement of the cycles and the diffusion speed of lithium ion is slower than that in 312nm film. This experiment proved that the cycleability and reversible capacity are depend on the film thickness.

However, thin film structure cannot decrease the stress induced by size effect on the horizontal direction, which also cannot avoid the material cracking, pulverization and loss contact with electrode. The cycle life is still too short for commercial use.

1.3.2.2 Nano Particle Anode

Silicon based nano particle can decrease the volume change level as well as enable the stress relaxation. Meanwhile, by reducing particle size into nanoscale, the diffusion length decreased which means the speed of electrochemical reaction increases compare with the thin film structure [13]. Liu, Zhong, Huang [14] discovered a strong size dependence of fracture by in situ transmission electron microscopy method. Their result shows there is a critical particle diameter of 150nm. The particles do not crack and fracture below this critical diameter.

Otherwise, the surface cracks initially occur on the particles, and results pulverization for the particles with the volume expansion. The reason is that the stored strain energy from the lithiation induced swelling is not sufficient to drive large cracks on small sized nanoparticles to resulting fracture. Thus, this kind of nano particles can keep the anode structures in the charge/discharge process which can improve the cycling performance.

But the size of nano particle is small because the particle diameter needs to be controlled around 150nm. This makes the contact surface area between anode and electrolyte is much smaller than other structures. Additionally, the electric capacity is small because of its small volume size.

1.3.2.3 Nanorod Anode

Since the poor reliability of thin film anode structure and the low electric capacity of nano particle structure, nanorod was invented to balance the reliability and capacity for anode which is illustrated in Fig.1.6.

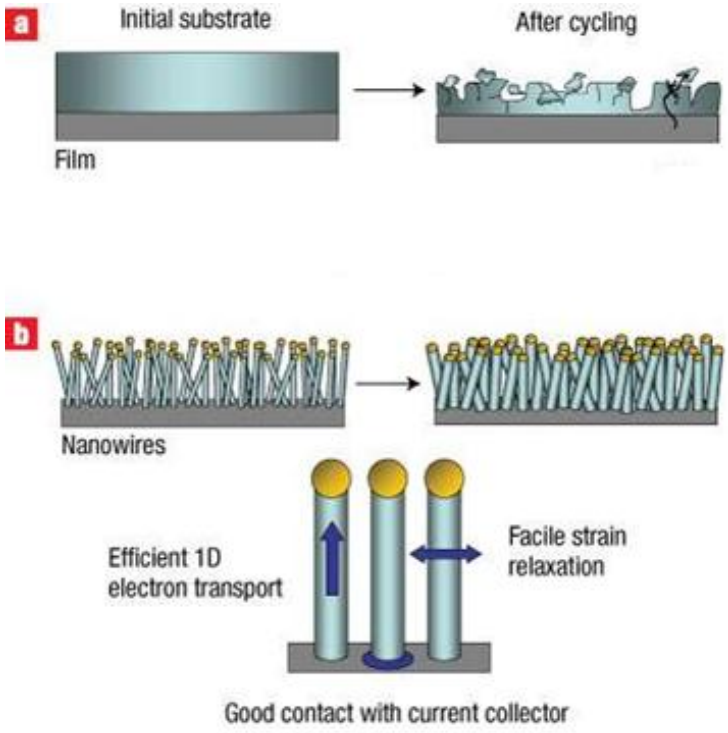

Figure1.6 Comparison between nano film and nanowires [15]

He, Yang et al [16] demonstrated a simple but versatile nanofabrication technique, termed dynamic shadowing growth (DSG). This technique employed a two-source electron beam deposition system which is capable to sculpture nanostructures with controlled morphologies structures and compositions. Different kinds of Si-based nanorods were fabricated to be compared the performances. 1: nanowire with intrinsic Si which is used as a control. 2: nanowire with multilayer Cu and Si which is designed to increase the conductivity of individual Si nanorods. 3: nanowire with Cu side-coated Si. The coating Cu on one side of Si nanorods is expected to both increase the conductivity of the Si nanorods and support the nanorods during volume expansion. 4: Uniform CuSi composite nanowire is used to target on the stress relaxation and enhance charge transfer performance. Experiment results showed that the intrinsic Si and composite nanostructures exhibit the best cycling performance with capacity retention of 60%-80% after 100 cycles of lithiation/delithiation process.

1.4 Motivations and objectives

1.4.1 Motivations

Lithium-ion batteries are one of the most popular electric energy storage devices and widely used in major areas such as portable electronics and EV. However, obviously today's graphite based lithium-ion battery cannot satisfy the rapidly growing power requirement due to the limited specific capacity (372mAh/g). For example, the smartphones cannot last long for frequent use and require daily charging. For EV, Tesla Roadster carries 6831 lithium ion cells which together weight half a ton (1100lb). Each cell weights equal around to a laptop one. However, so many cells can only cover a distance of about 220 miles, which is around half the driving distance of a fully loaded gasoline vehicle. With the rapidly increasing demand for higher capacity rechargeable batteries, researchers from all over the world are looking for ways to enhance the battery performance with higher energy density, longer battery life and lower cost. For this reason, silicon has most recently become a popular research topic because it has the

highest-known theoretical specific capacity of approximately 4200 mAh/g, which is 10 times that of the graphite anodes. Also, it is the second most abundant element on the earth, However, silicon experiences large volume change up to 400%, which may induce very high stress. The previous researches showed that the problem can be mitigated by incorporating other compositions and tailoring Si into nanostructures such as nanorods. For nanorods, the huge difference of deformations between the substrate and rods can still damage the anodes.

1.4.2 Objectives and Approach

The objectives are to examine the stress state in a CuSi composite nanorod during lithiation/delithiation and to gain insights in how to design such nano-anodes with improved performance against adverse stress effects. In the present thesis, a composition-graded CuSi nanorod is examined. The model is that the bottom substrate is pure copper and the top is pure silicon nanorod, and between them is a grading zone with Cu % gradually decreasing meanwhile Si % increasing from bottom up. This structure design is intended to target the ripping-off of nanorods from a substrate through gradual stress relaxation. Parametric study is carried out to show how the stress varies with the grading zone length. The model takes into account nonlinear effects of elastoplasticity, finite strain and finite rotation. The finite element software Mechanical APDL (ANSYS) 13.0 is employed to numerically carry out the analysis.

CHAPTER 2

PROBLEM FORMULATION

This chapter introduces the theory of this project and what the ANSYS simulation is based on. The constitutive stress-strain relationships are described first. After that, a brief introduction of Von Mises criterion for plastic yielding is given. Finally, the chemical and plastic strains are discussed.

2.1 Overall Strain

In this project, the model material undergoes large deformations. Silicon material can expand up to 400 % of its initial volume when fully lithiated.

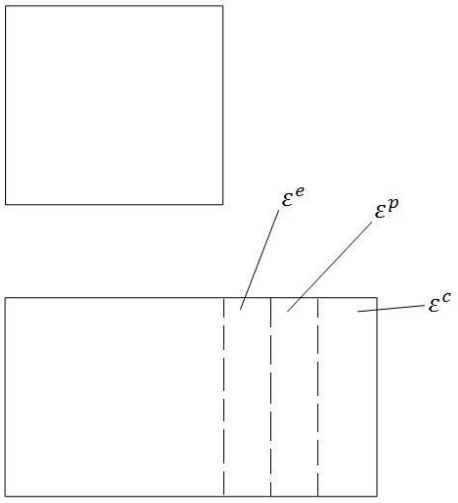

Figure 2.1 Strain Compositions

As schematically illustrated in Fig. 2.1, the total strain ε is partitioned in three terms.

$$\varepsilon = \varepsilon^e + \varepsilon^p + \varepsilon^c \tag{2.1}$$

They are elastic, plastic and chemical strains, respectively. Generally, the overall charging process on the nanorod is considered to be elastoplastic. The material is linearly elastic before

the yielding point, so that stresses can be calculated by knowing strains and elastic constants. Since plastic strain ε^p is treated as large, deformation and stress are history-dependent after yielding. Plastic strains make materials have permanent deformation and shape change. Hence, the final results would be different to a particular final loading state from different histories. In the battery case, the first time charging process is simulated. In the theoretical calculation, history is considered by formulations based on increments of stresses and strains. Therefore, the incremental version of Eq. (2.1) is given by

$$\{d\varepsilon\} = \{d\varepsilon^e\} + \{d\varepsilon^p\} + \{d\varepsilon^c\} \tag{2.2}$$

The elastic strain ε^e is treated as small, on the other hand, the chemical strain ε^c and plastic strain ε^p are considered to be large. Besides, the elastoplastic model assumes bilinear isotropic hardening. These terms are described separately below.

2.2 Elastic Stress-strain Relationship

We consider a nanorod experiencing stresses induced by the volume expansion during the charging process. The material we discuss here are linearly elastic and isotropic, below yielding point. The incremental stress is related to the incremental elastic strain by:

$$d\{\sigma\} = [E] * d\{\varepsilon^e\} \tag{2.3}$$

Where:

$d\{\sigma\} = stress\ vector = d\left[\sigma_x\ \sigma_y\ \sigma_z\ \tau_{xy}\ \tau_{yz}\ \tau_{xz}\right]^T$

$[S] = elastic\ \ stiffness\ matrix$

$d\{\varepsilon^e\} = d\left[\varepsilon_x\ \varepsilon_y\ \varepsilon_z\ \gamma_{xy}\ \gamma_{yz}\ \gamma_{xz}\right]^T$

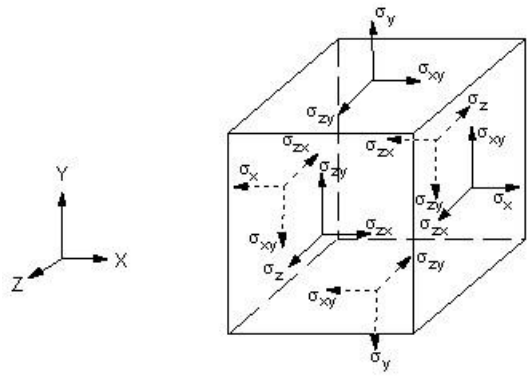

Figure 2.2 Stress Tensor Definition

So Eq. (2.3) could be inverted to:

$$d\{\varepsilon^e\} = [S]^{-1} * d\{\sigma\} \tag{2.4}$$

where the elastic compliance matrix is given by:

$$[S]^{-1} = \begin{bmatrix} 1/E & -\upsilon/E & -\upsilon/E & 0 & 0 & 0 \\ -\upsilon/E & 1/E & -\upsilon/E & 0 & 0 & 0 \\ -\upsilon/E & -\upsilon/E & 1/E & 0 & 0 & 0 \\ 0 & 0 & 0 & 1/G & 0 & 0 \\ 0 & 0 & 0 & 0 & 1/G & 0 \\ 0 & 0 & 0 & 0 & 0 & 1/G \end{bmatrix} \tag{2.5}$$

where υ is the Poisson ratio, E is the Young's Modulus and G is the shear modulus of material. This matrix is for isotropic material.

2.3 Von Mises Criterion for Yielding

In this project, the model bears tremendous volume expansion, which is expected to induce plastic strain ε^p. The Von Mises criterion, also called the distortion-energy theory, is applied to determine the yield surface here. This theory indicates that yielding occurs when the distortion strain energy equals to or exceeds a threshold, which is briefed as follows.

The total elastic strain energy U is divided in two terms:

$$U = U_v + U_d \tag{2.6}$$

where U_v is the strain energy per unit volume due to volume change, and U_d is the strain energy per unit volume due to distortion. They are expressed in terms of principal stresses, $\sigma_1, \sigma_2, \sigma_3,$ as follows:

$$U = \frac{1}{2E}[{\sigma_1}^2 + {\sigma_2}^2 + {\sigma_3}^2 - 2\upsilon(\sigma_1\sigma_2 + \sigma_2\sigma_3 + \sigma_3\sigma_1)] \tag{2.7}$$

$$U_v = \frac{1-2\nu}{6E}(\sigma_1 + \ \sigma_2 + \sigma_3)^2 \tag{2.8}$$

$$U_d = \frac{1+\nu}{3E}\left[\frac{(\sigma_1-\sigma_2)^2 + (\sigma_2-\sigma_3)^2 + (\sigma_3-\sigma_1)^2}{2}\right] \tag{2.9}$$

For uniaxial tension, at yielding, $\sigma_1 = \sigma_y$, and $\sigma_2 = \sigma_3 = 0,$ and the distortion energy becomes

$$U_d = \frac{1+\nu}{3\mathrm{E}}{\sigma_y}^2 \tag{2.10}$$

The von Mises criterion for yielding requires

$$\left[\frac{(\sigma_1-\sigma_2)^2 + (\sigma_2-\sigma_3)^2 + (\sigma_3-\sigma_1)^2}{2}\right]^{1/2} \geq \sigma_y \tag{2.11}$$

The left-hand side of equation 2.11 is termed the von Mises stress σ'., given in terms of principal stresses $\sigma_1, \sigma_2, \sigma_3$. Figure 2.3 shows the projection of the von Mises yield criterion into the σ_1, σ_2 plane. In general expression of a stress state, the Von Mises criterion is given by

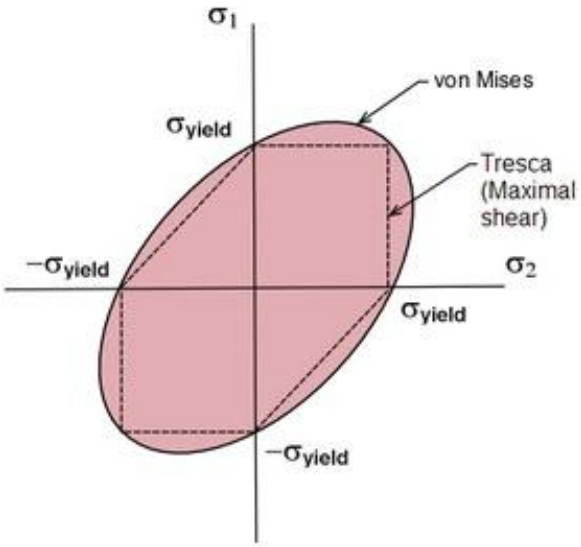

Figure 2.3 von Mises criterion [17]

By using x, y, z components of 3-D stresses, the von Mises stress can be written as

$$\sigma' = \frac{1}{\sqrt{2}}\left[(\sigma_x - \sigma_y)^2 + (\sigma_y - \sigma_z)^2 + (\sigma_z - \sigma_x)^2 + 6(\tau_{xy}^2 + \tau_{yz}^2 + \tau_{zx}^2)\right]^{1/2} \geq \sigma_y \tag{2.12}$$

2.4 Chemical Strain

During lithiation, Lithium ions come into the anode material and chemically react with it. Thus, chemical strain should be included, which is given by

$$d\{\varepsilon^c\} = \gamma\{I\}dc \tag{2.13}$$

where γ is the chemo-expansion coefficient, c is the Lithium-ion concentration, and {I} is the identity matrix. It is assumed that the chemical expansion is isotropic.

2.5 Relations Between dε and dσ

The bilinear isotropic elastoplastic model along with the von Mises criterion is applied in this project. Within the yield surface, there would occur only elastic strain. According to Eq.2.2 and Eq.2.3, the increments of stress for elastic stresses before yielding are

$$\{d\sigma\} = [E]\{d\varepsilon - d\varepsilon^c\} \tag{2.14}$$

After the stress exceed the yielding point, the plastic strain increment is given by

$$\{d\varepsilon^p\} = \left\{\frac{\partial Q}{\partial \sigma}\right\} d\lambda \tag{2.15}$$

Where Q is called plastic potential which is equal to the von Mises yield surface F in this project, $d\lambda$ is plastic multiplier which is a scalar, and can be got from textbook [12]

$$d\lambda = [P_\lambda]\{d\varepsilon\} \tag{2.16}$$

Where $[P_\lambda]$ is a row matrix

$$[P_\lambda] = \frac{\left\{\frac{\partial F}{\partial \sigma}\right\}^T [E]}{\left\{\frac{\partial F}{\partial \sigma}\right\}^T ([E] + \eta[C]) \left\{\frac{\partial F}{\partial \sigma}\right\} + (1-\eta) H_p} \tag{2.17}$$

Where H_p is the strain hardening ratio, η denotes to a "mixed" hardening rule which includes both isotropic and kinematic hardening, $0 < \eta < 1$. Hardening is pure isotropic if $\eta = 0$ and purely kinematic if $\eta = 1$. In this project the hardening is pure isotropic, so $[P_\lambda]$ can written as

$$[P_\lambda] = \frac{\left\{\frac{\partial F}{\partial \sigma}\right\}^T [E]}{\left\{\frac{\partial F}{\partial \sigma}\right\}^T [E] \left\{\frac{\partial F}{\partial \sigma}\right\} + H_p} \tag{2.18}$$

Besides, $\left\{\frac{\partial F}{\partial \sigma}\right\}$ is given by

$$\left\{\frac{\partial F}{\partial \sigma}\right\} = \frac{3}{2\sigma_0}\{s_\sigma\} \tag{2.19}$$

Where σ_0 is the largest von Mises stress reached in the previous plastic strain, and s_σ is the deviatoric stress which equals the actual normal stresses minus the mean normal stress σ_m.

From Eq.2.14 and Eq.2.15, we can obtain

$$\{d\sigma\} = [E]\left(\{d\varepsilon\} - \left\{\frac{\partial F}{\partial \sigma}\right\} d\lambda\right) \tag{2.20}$$

Substituting Eq.2.17 into Eq.2.20 provide

$$\left[E_{ep}\right] = [E]\left([I] - \left\{\frac{\partial F}{\partial \sigma}\right\}[P_\lambda]\right) \tag{2.21}$$

Where $\left[E_{ep}\right]$ is the effective stiffness matrix. Before the yield surface is reached, $\left[E_{ep}\right]$ equals to $[E]$. Thus, the elastic-plastic stress-strain relationship can be written as

$$\{d\sigma\} = [E_{ep}]\{d\varepsilon - d\varepsilon^c\} \tag{2.22}$$

Where $\left[E_{ep}\right]$ is the combination of Eq.2.18 and Eq.2.21

$$\left[E_{ep}\right] = [E]\left([I] - \left\{\frac{\partial F}{\partial \sigma}\right\}\frac{\left\{\frac{\partial F}{\partial \sigma}\right\}^T [E]}{\left\{\frac{\partial F}{\partial \sigma}\right\}^T [E]\left\{\frac{\partial F}{\partial \sigma}\right\} + H_p}\right) \tag{2.23}$$

Combining Eq.2.22 into Eq.2.23 provide

$$\{d\sigma\} = \left([E] - \frac{[E]\left\{\frac{\partial F}{\partial \sigma}\right\}\left\{\frac{\partial F}{\partial \sigma}\right\}^T [E]}{\left\{\frac{\partial F}{\partial \sigma}\right\}^T [E]\left\{\frac{\partial F}{\partial \sigma}\right\} + H_p} \right) \{d\varepsilon - d\varepsilon^c\}$$

(2.24)

CHAPTER 3

ANSYS MODELING

The above elastoplastic problem can be solved numerically by applying the finite element method. A finite element model of a grading nanorod with substrate is developed to validate the idea in objective. The commercial finite element software ANSYS is used to develop the required model. In this chapter, details of the model geometry, material property and theories will be demonstrated. Then, the chapter also shows the modeling procedures, loading and boundary conditions which applied on the model. After that, a reduced model will be developed by using the same script, and its results will be compared with the analytical solution to verify the validity of the script.

3.1 ANSYS Model Development

3.1.1 Geometry

In realistic, thousands of the nanorods attach on the substrate in anode electrode. Here, only one nanorod with substrate is developed. As figure 4.1 shows, the 100% copper part is the substrate which can conduct electricity and attach the silicon nanorods. The middle CuSi part is the compound grading zone which is important to buffer the induced stress by huge volume change because of charging. The top part is the 100% silicon rod which captures the lithium ion and stores the energy.

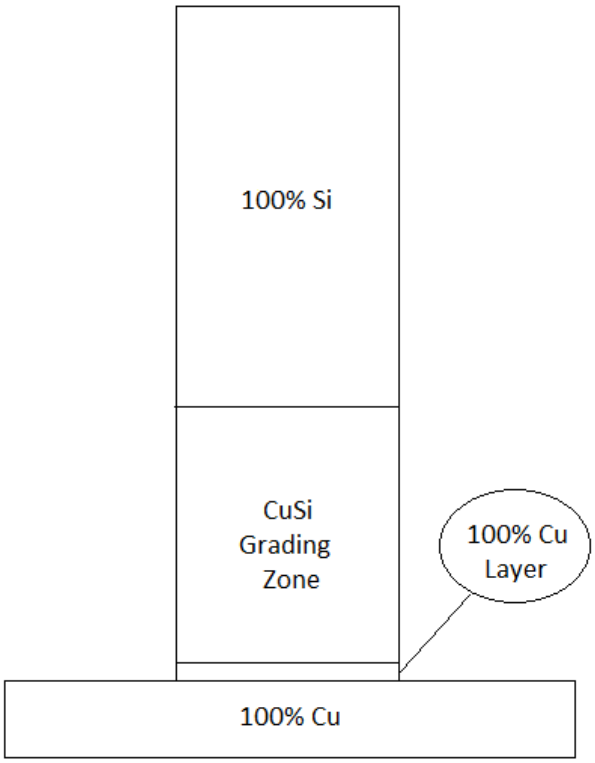

Figure 3.1 Nanorod geometry

Consider an axisymmetric nanorod is developed. The dimensions are all normalized by radius of nanorod, R, to avoid the errors due to the nano scale numbers. The dimension of the nanorod can be seen in Table 3.1

Table 3.1 Dimension of the nanorod

Part	Radius	Length
Pure copper substrate	2R	0.5R
Pure copper grading layer	1R	0.2R
Whole nano rod	1R	4R
CuSi grading	1R	By Compare

3.1.2 Material properties

In this project, material properties are all defined as bilinear isotropic. Because computational errors would occurs in nano to micro scales, all the stresses and material properties are normalized by Young's modulus of Silicon, E_{Si}. It needs to be clarified that this chemical stress problem is mathematically identical as a thermal stress problem. So the chemical lithiation process is treated as a thermal process in the ANSYS simulation. There are two processes for the model. Before charging, the material properties are given as follows,

$$E_{Si} = 1, \qquad E_{Cu} = 0.8$$

$$\alpha_{Si} = 0.40546, \qquad \alpha_{Cu} = 1 * 10^{-37}$$

$$\upsilon_{Si} = 0.3, \qquad \upsilon_{Cu} = 0.3$$

$$\sigma'_{Si} = 0.03, \qquad \sigma'_{Cu} = 0.0006$$

$$H_{Si} = 0.1, \qquad H_{Cu} = 0.05$$

Where the suffix notation "Si" represents the material of Silicon, "Cu" represents Copper. *E* are the Young's Modulus. α is the chemical expansion coefficient. υ is the Poission ratio. *H* is the hardening ratio.

During the lithiation process, Lithium-ions come into the battery anode and react with Silicon rods. The material property of the compound is

$$E_{SiLi} = 0.22575$$

$$\alpha_{SiLi} = 0.40546$$

$$\upsilon_{SiLi} = 0.3$$

$$\sigma'_{SiLi} = 0.03$$

$$H_{SiLi} = 0.05$$

The Young's modulus of SiLi above is for fully concentration state. Since after the fully reaction, each Silicon atom can capture 4.4 Lithium ions to form compound $\mathrm{Li_{22}Si_5}$. Yang [13] has showed the Young's modulus of $Li_{22}Si_5$ is about 40GPa in his previous work.

3.1.3 Modeling

Assigning material properties and defining element type are necessary in ANSYS. Since the model is axisymmetric, both PLANE182 and 183 can be worked in this case. PLANE182 is called 2D 4nodes structural solid element. This element can be used as plane element or axisymmetric element and defined by four nodes which all have two degrees of freedom in nodal x and y directions. PLANE182 can simulate the problem such as plasticity, hyperelasticity, large deformation and large strain. For PLANE183, it has the same features as PLANE182, but it is the higher order element with 8 nodes. Because the nanorod doesn't have complicated geometry, PLANE182 is enough to be used for simulation. This also makes the model simple and reduces the time of computational calculation. The modeling and mesh procedures are shown as follow

1. List the material properties and geometry properties which are show in previous
2. Define 2D 4nodes PLANE182 as element type. The model is axisymmetric by y-axis as default
3. Modeling process is divided by two. First is modeling and meshing the pure copper substrate and pure copper rod layer. Second, the nanorod including CuSi grading zone and pure silicon zone are developed and meshed. After finish the above two parts, all the elements are combined together.
4. To modeling the substrate and copper layers, 6 key points are assigned. Then area is defined by those key points which figure 3.2 shows

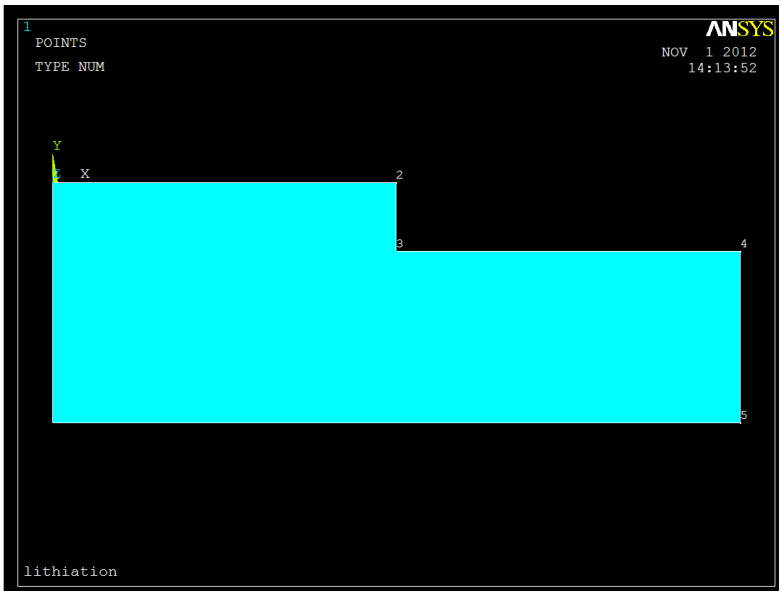

Figure 3.2 Substrate area

5. Corner keypoint 3 is at the concentration in the simulation. Spider web shaped mesh need be defined. This kind of mesh is useful for modeling stress concentrations and crack tips. Define keypoint 3 as a concentration keypoint about which the substrate area mesh will be skewed. After that, the general 2D area mesh is defined. To create the general mesh, the line is picked and the size of divided element is specified. In this case, element size is defined as dy, thus everything will be parametric connected with the size. The meshed elements are PLANE182 elements. Then the meshing is mapped as shown below

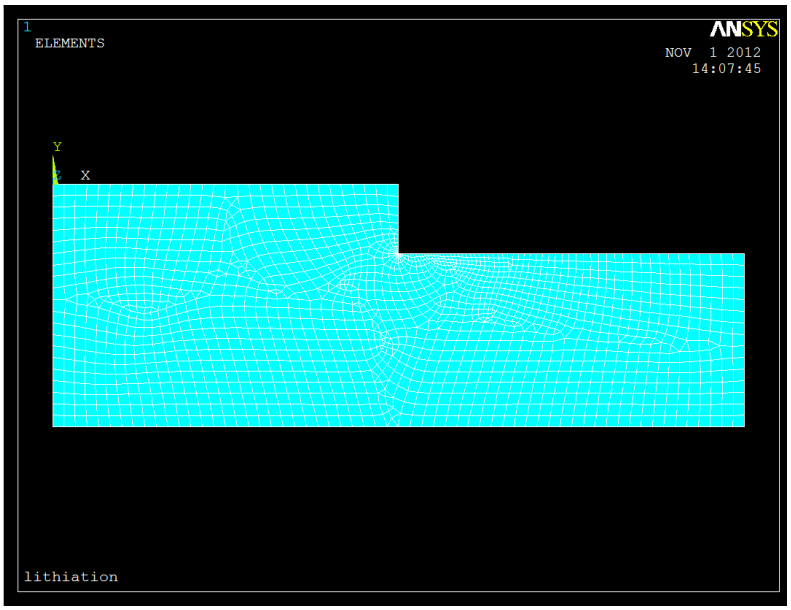

Figure 3.3 Mesh in substrate area

6. Define the material properties of copper in this area by using the listing numbers from the very first step. Then the substrate part is finished.
7. The nanorod part is modeled layer by layer from the top of the substrate which is showed as figure 3.4.

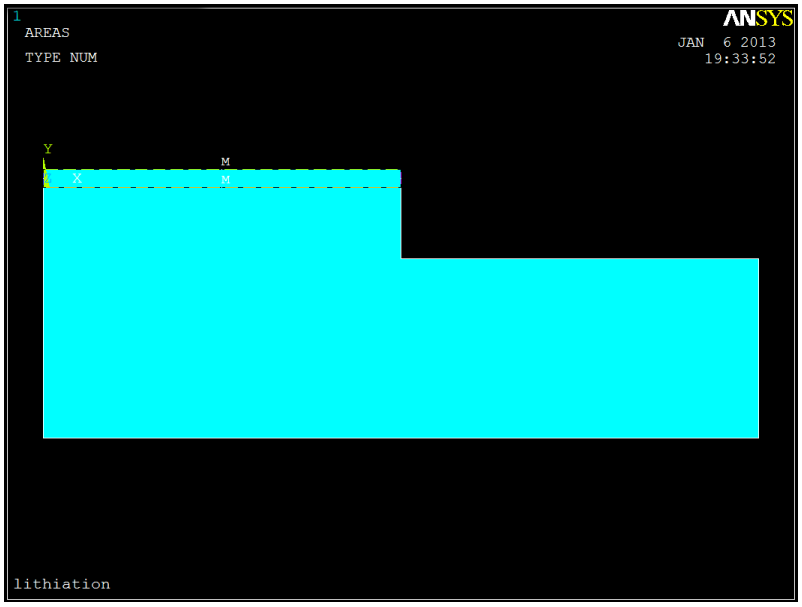

Figure 3.4 First layer of the nanorod

A if function is created to determine the layer locates in grading zone or in pure silicon zone. In CuSi compound grading part, the bottom has the property of 100% copper; the top has the property of 100% silicon. Between pure silicon part and pure copper part, each layer is added by a constant difference, which means the material properties in grading zone linearly changes. Then pick the line to mesh by the mesh size which previously defined. After the grading zone, the layers are defined as the pure silicon property with no property changes.

8. Silicon reacting with lithium-ion to form SiLi compound during the charging process causes the changes of material properties of nanorod. Since the chemical source is treated as thermal source in ANSYS as mentioned before, temperature goes up represents the lithiation process. The materials in nanorod are defined as temperature-dependent. So when original and final states are defined, all material properties for every layer will be interpolated by computer with temperature change.
9. All the nodes and keypoints are merged together to form as a whole entity. See Figure 3.5

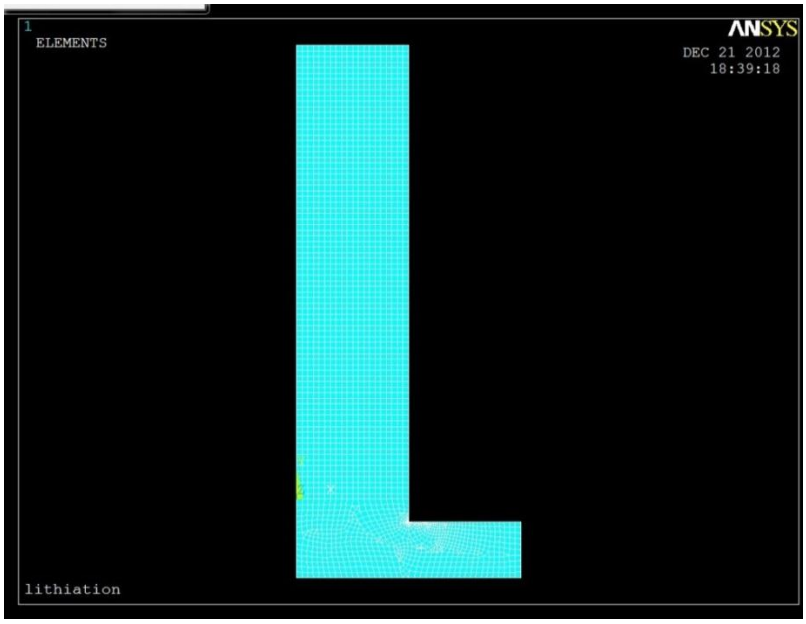

Figure 3.5 Model entity

10. To set boundary condition, the bottom line of the substrate is selected to constrain on vertical direction. Which means the constraint on substrate is equal to a roller which is free horizontally but fix vertically.
11. In the earlier simulation, material overlaps were observed at the corner between the rod and substrate because of the large deformation. Therefore, two lines near the corner will defined as contacts which is showed as figure 3.6

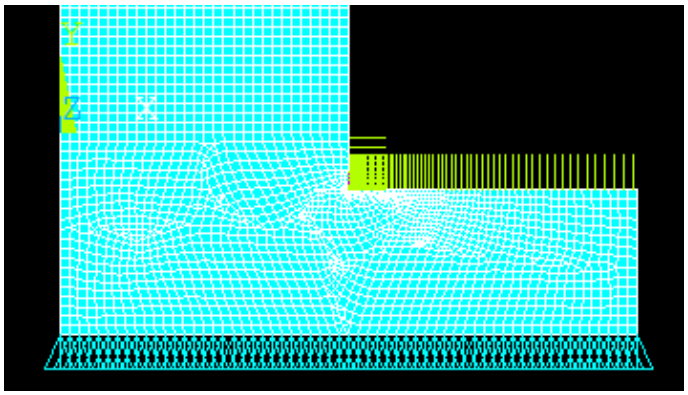

Figure 3.6 Defining line contacts

12. Temperature loading are set to increase from 0 to 1 and divided by 50 time steps. We defined that the concentrations of lithium are represented by the temperature in this simulation. So when temperature is 1 means the model is in fully concentrate state that each silicon atom captured 4.4 Li-ions; when temperature is 0 means the model is in initial state which is before lithiation. All the elements in the model are assigned 0.02 temperature increment by each time step until the 50th.
13. Turn on the geometrical nonlinearity switch to accommodate the larger deformation in this case.

3.2 Validation of FEM Model

Since analytical solution is not easy to get to compare with the finite element solution in this complicated case. So a reduced model is developed by the same script as the non-reduced model, and the comparison of analytical solution and finite element solution are performed.

The reduced model contains one material which is silicon, so we can treat it as the top part of the previous grading model. The material properties are not temperature-dependent in the reduced model. Besides, the material property is assumed without yielding. Thus, this becomes to an elastic stress-strain problem. In this case, the boundary condition is that top and bottom edge are constrained vertically, but free in horizontal direction. The loading keeps the same which the temperature goes from 0 to 1 by 50 time steps. The simulation plot is shown in figure 3.7

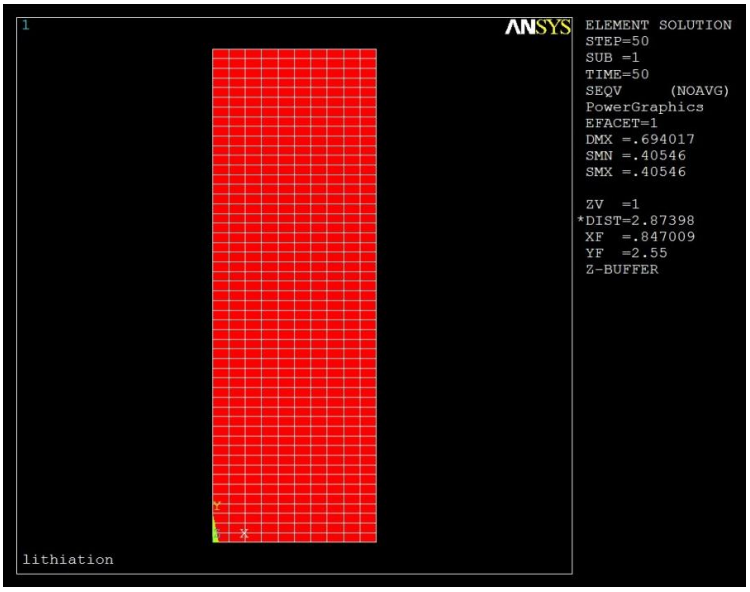

Figure 3.7 Reduced model

In analytic way, the coordinate system is transferred to polar coordinate first because the model is axisymmetric.

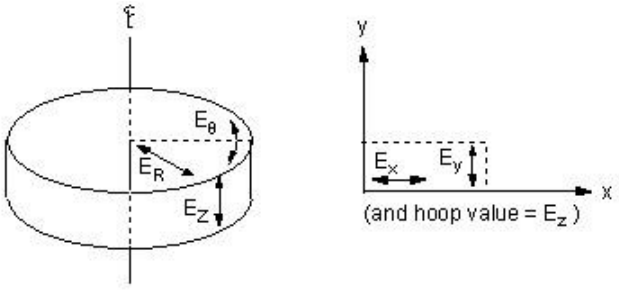

Figure 3.8 Material coordinate systems

As Figure 3.8 shows, x-y-z coordinate system can be transferred to R-θ-Z cylindrical system. Thus, $R \to x$, $\theta \to z$, $Z \to y$. Rearranging equation 2.5 to match polar coordinates yield

$$\varepsilon_r{}^e = \frac{\sigma_r}{E} - \nu\frac{\sigma_\theta}{E} - \nu\frac{\sigma_z}{E}$$

$$\varepsilon_\theta{}^e = \frac{\sigma_\theta}{E} - \nu\frac{\sigma_r}{E} - \nu\frac{\sigma_z}{E}$$

$$\varepsilon_z{}^e = \frac{\sigma_z}{E} - \nu\frac{\sigma_r}{E} - \nu\frac{\sigma_\theta}{E}$$

(3.1)

Combining equation 3.1 and equation 2.10:

$$\varepsilon_r = \frac{1}{E}[\sigma_r - \upsilon(\sigma_\theta + \sigma_z) + \alpha T]$$

$$\varepsilon_\theta = \frac{1}{E}[\sigma_\theta - \upsilon(\sigma_r + \sigma_z) + \alpha T]$$

$$\varepsilon_z = \frac{1}{E}[\sigma_z - \upsilon(\sigma_r + \sigma_\theta) + \alpha T]$$

(3.2)

In this particular case, the model is constrained in z direction and free along the radius which gives

$$\varepsilon_z = 0$$

$$\sigma_\theta = \sigma_r = 0$$

The temperature loading is T=1. Appling the boundary condition and loading into Equation 3.2 and get

$$0 = \frac{1}{E} * \sigma_z + \alpha$$

(3.3)

After substituting the normalized silicon material properties, stress σ_z is equal to 0.40546 which is the same as the finite element solution.

CHAPTER 4

Results and Discussion

In this chapter, several trials of simulation with different grading length are performed. The results of selected nodes are discussed and compared with each other. Figures and plots are also showed after.

4.1 Results Discussion for Grading Length Lc=1

The snapshot showed below is when the simulation is done at 50th time steps which mean the nanorod is in the state of fully charged. The mesh size of 30*30 elements per square length is applied which was verified to yield relatively accurate results.

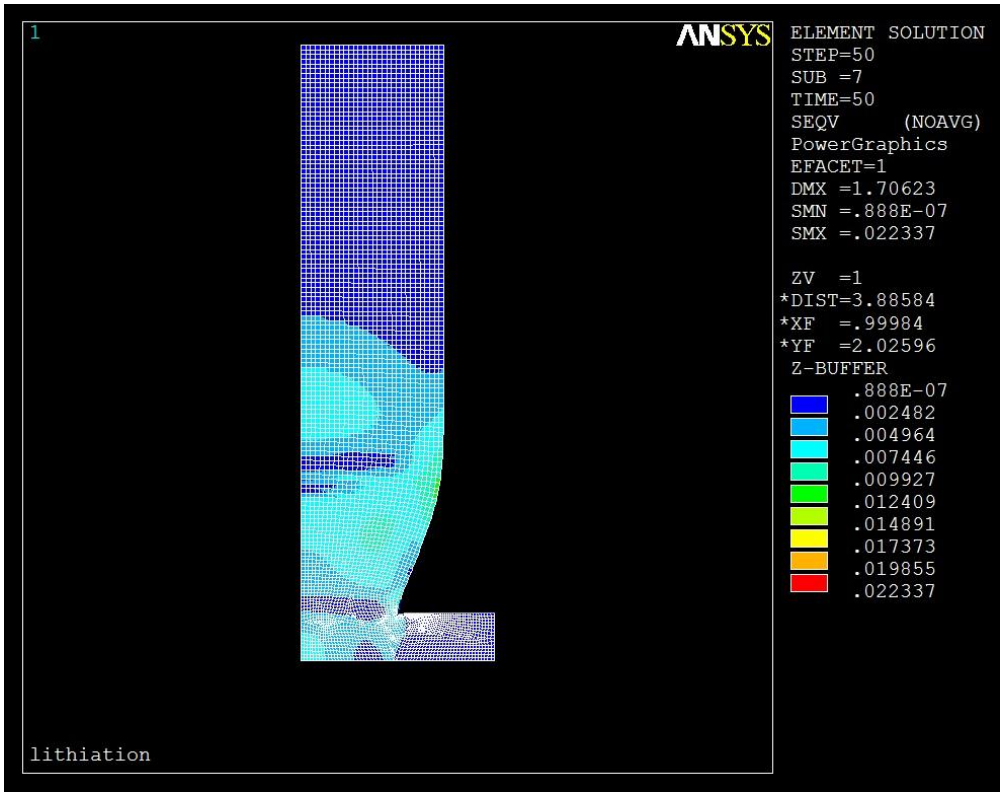

Figure 4.1 fully charged state

The grading length is Lc=1 for Figure 4.1. From the figure, the pure silicon part has significant shape expansion due to the material property. So the volume change is highly non-uniform although the loading is uniform applied. The contours of different colors are about the von Mises stress. The highest con Mises stress located on the surface of materials transition between the grading zone and pure silicon section. The following figure shows the morphological changes at various stages along with the increasing of time.

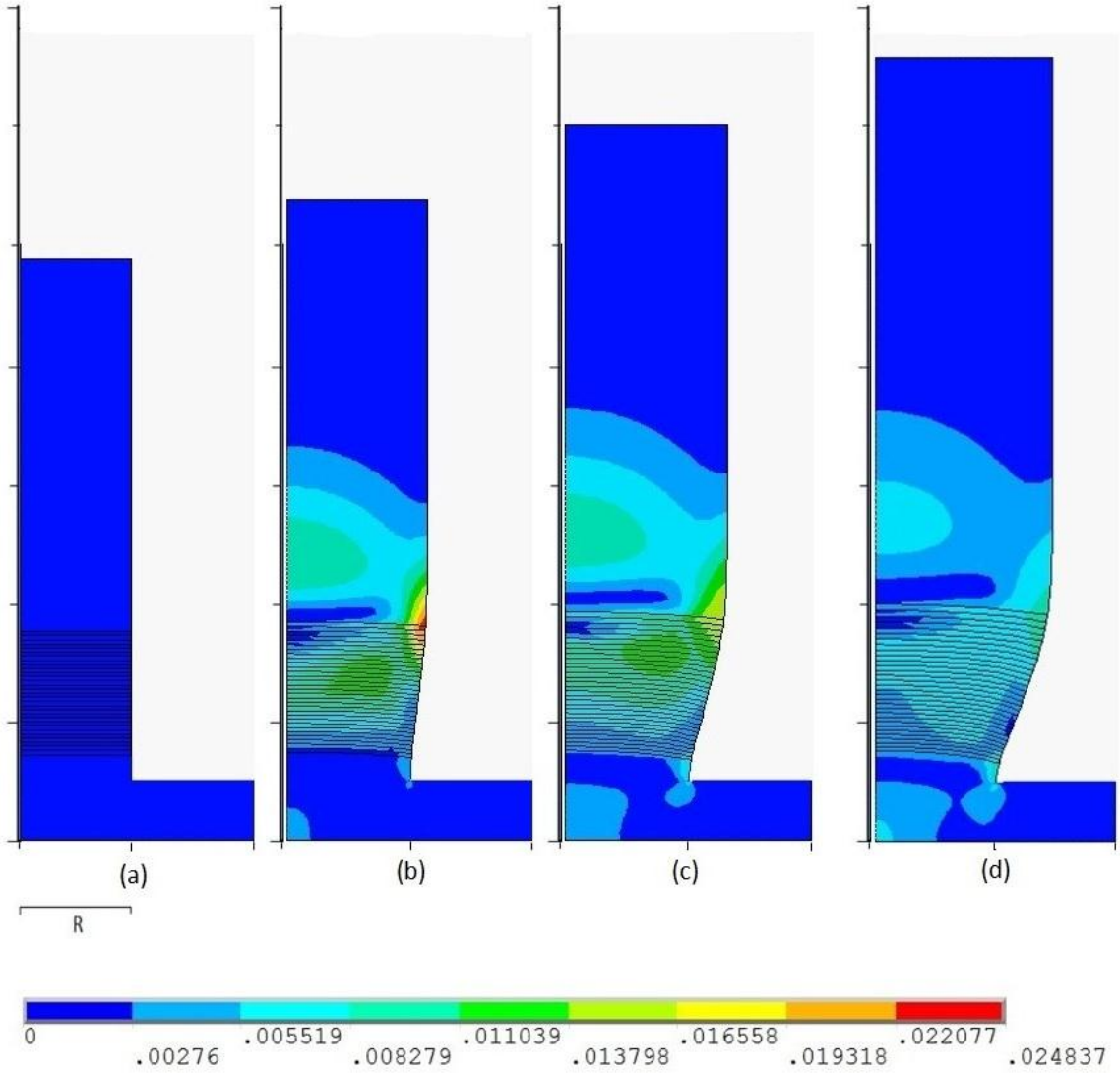

Figure 4.2 Isotropic contour plots of von Mises stress at different time points.

(a) Initial condition (b) 20% concentration (c) 60% concentration (d) fully concentration

In above figure, the space between the two adjacent ticks is equal to one unit of length which is defined as R here. Figure 4.2(a) is the initial state when the load has not applied on the model; (b) is the critical state which the von Mises stress reaches to the highest when in 20% Li concentration; (c) is in the state when the concentration of Li-ion equals to 60%; (d) indicates the finial state which the nanorod is fully charged. After the nanorod is fully lithiated, the upper pure silicon part expanded around 50% on both vertical and horizontal directions. So the total volume expansion of silicon rod closely equal to 338% which is within expectation. For the whole model, the total volume expansion is around 254%.

From Figure 4.2, the pure copper substrate barely changed in size but the silicon rod gradually expend due to the thermal expansion coefficient of silicon is much higher than copper. Due to the huge difference of the deformation in the model, stresses are induced. There is no stress concentration on the top silicon part is because the top end is free for material expansion. From (b), (c), (d), it can be seen that there grows up significant tensile stress on the nanorod surface of the transition section. Besides, Figure 4.3 shows stresses also concentrate in the middle of the grading zone and the corner between the nanorods and the copper substrate. Therefore, cracks may first occur at the surface of transition part, and detachment between anode rod and collector would occur due to the stress concentration in cyclic charging.

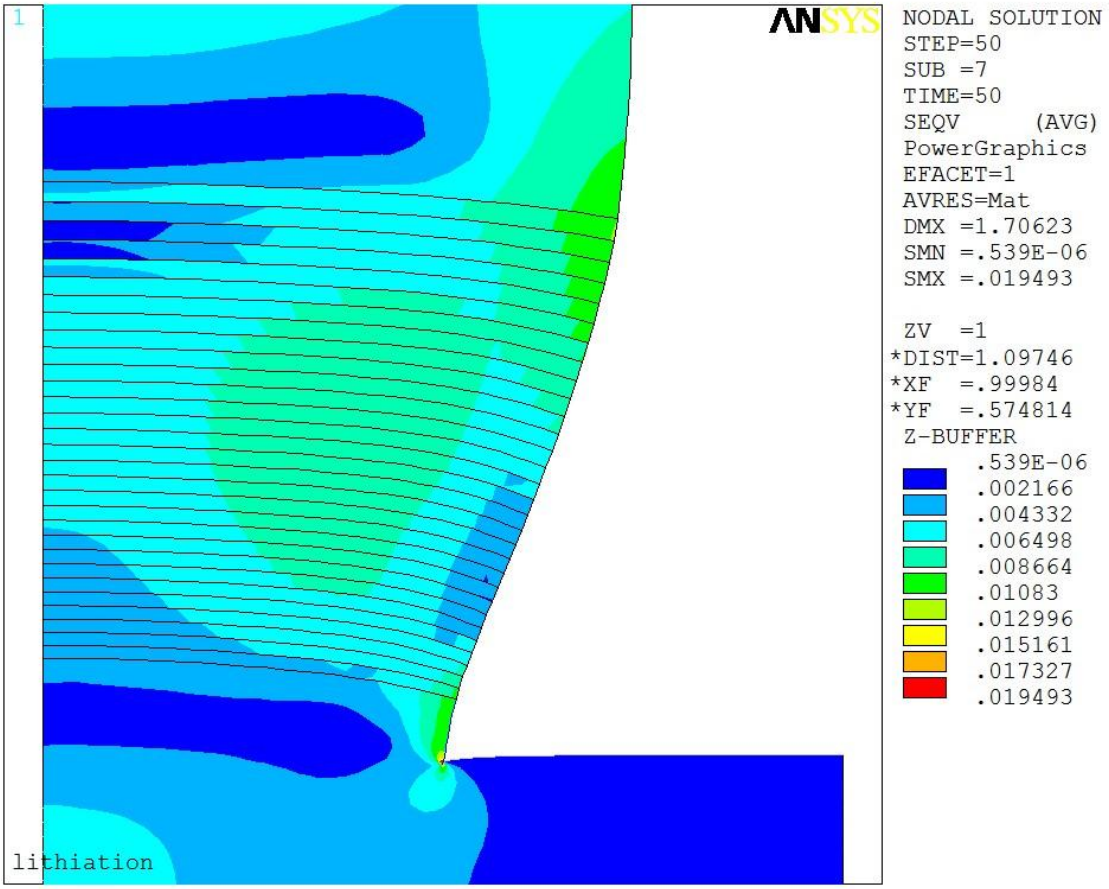

Figure 4.3 Zoom-in plot for grading zone

4.2 Discussion for Different Lengths of Grading Zone

To further study the stresses in a silicon based nanorod with grading, six sets of simulations with different grading length are performed. The grading length, Lc, equals to 0.5R, 1R, 1.5R, 2R, 2.5R, 3R respectively and R is the unit of length in this simulation. The nodal solutions which have the maximum von Mises stress in each set are selected to compare with each other. Besides, the node in the corner of material transition section also has the stress concentration. So the stresses comparison is also performed.

4.2.1 Comparison of Maximum von Mises Stresses

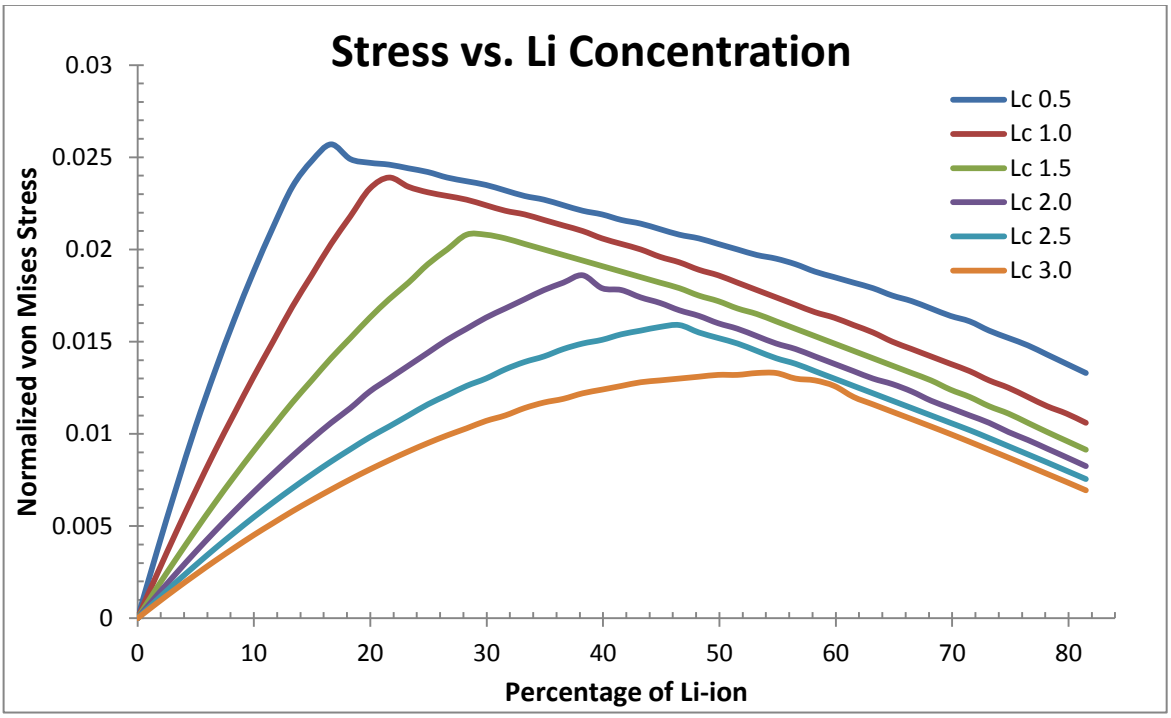

Figure 4.4 Comparisons of Max Stresses for Different Cases

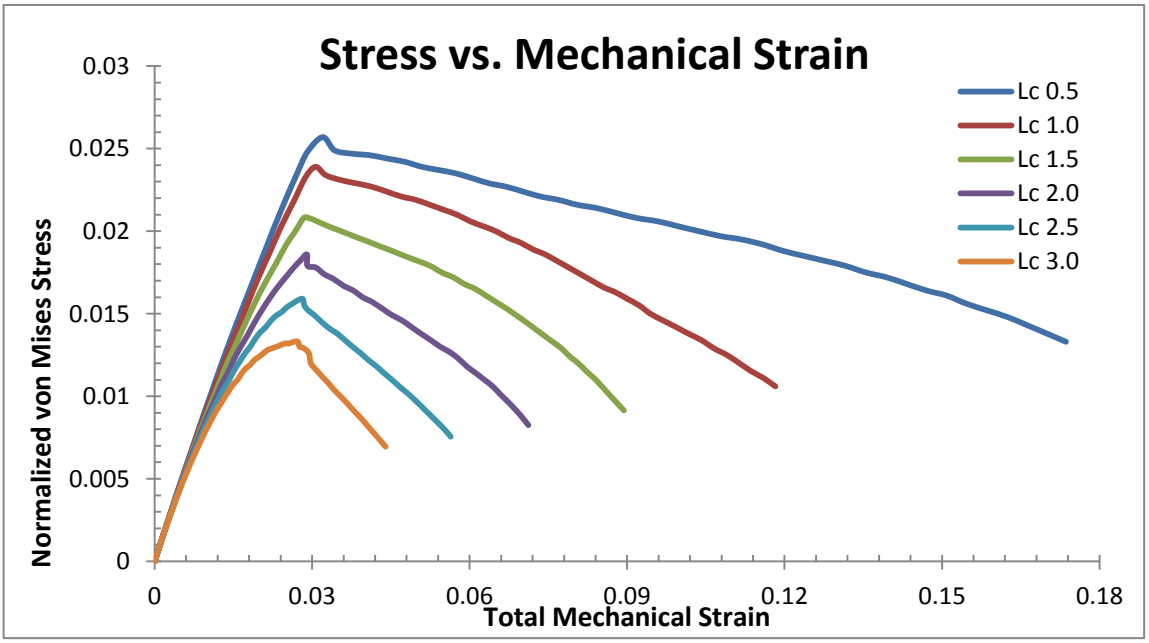

Figure 4.5 Stress-strain Relation

Among these six cases, the maximum von Mises stresses all locate on the surface nodes of material transition part between grading zone and pure silicon part. From figure 4.4, each case shows that the stress increase with curvature until its yielding point, and then drops. Recall that the model materials are defined as bilinear isotropic material properties in previous. Suppose the material concentrations are constant, the stress would linearly increase until yielding, and then linearly increase by a small slope. The reason why the stresses perform as figure 4.4 shows instead of bilinear is that the modulus of the LiSi compound changes during the lithiation process. In theory, lithium-ions react with silicon atoms during the charging process, and each silicon atom can capture 4.4 lithium-ions. So the percentage of silicon atoms in the upper silicon rod would drop from 100% to 18.5% until fully charged. As we know, the modulus of lithium is much lower than that of silicon. During the process of the chemical reaction between silicon and lithium, the modulus of the anode rods actually decreases. In this project, material properties are set as temperature-dependent. The initial and final properties are firstly defined, and ANSYS would linearly interpolate between the two values which means the concentration of lithium-ions is assumed to linearly increase in the model. Therefore, the plots of stresses are curved shape and the stresses drop after yielding. Comparing all the six cases in the plot, stress and the yielding point decrease when increasing the grading length. The case of Lc 3.0 reached its yielding point when concentration of Li-ion is 55%, but the case of Lc 0.5 yielded when Li-ion is only 17%. This means the rod of low grading length would yield earlier than that of high grading length in actual charging process. The yielding points decrease is also caused by the increments of Lithium concentration because the yielding point of Li is much lower than that of Silicon. Although the longer grading length has lower yielding point, it actually can last longer before yielding. The Fig 4.5 shows the stress-strain relation where the strains include both elastic and plastic strains. Since the case of shorter grading length bears more induced stresses, the material is driven to have more strains which have larger deformations. After yielding, materials are easy to drive for expand. We can see that the final strain of Lc 0.5 is

about 4 times larger than that of Lc 3.0 after yielding. Besides, the locations of same stains correspond to different stresses is because different Li concentrations have different material properties.

4.2.2 Comparison of the stresses at corner node.

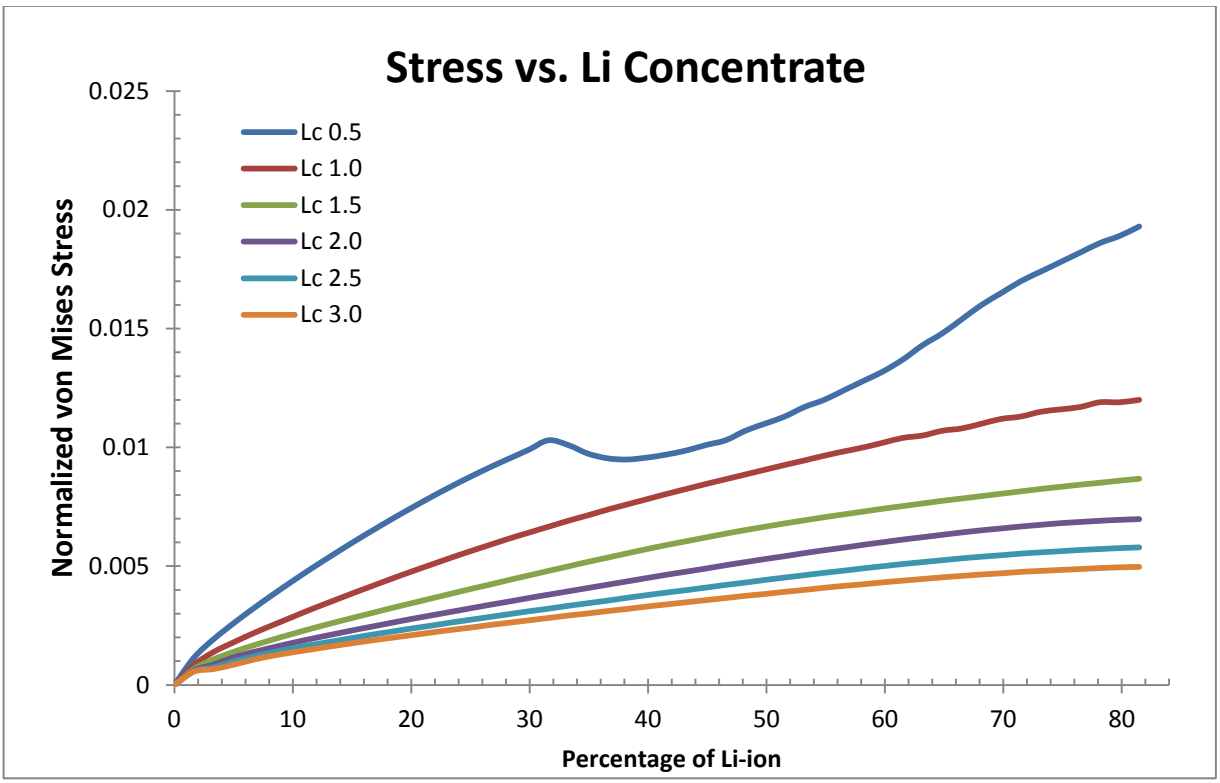

Figure 4.6 Nodal Solutions in corner node for different cases

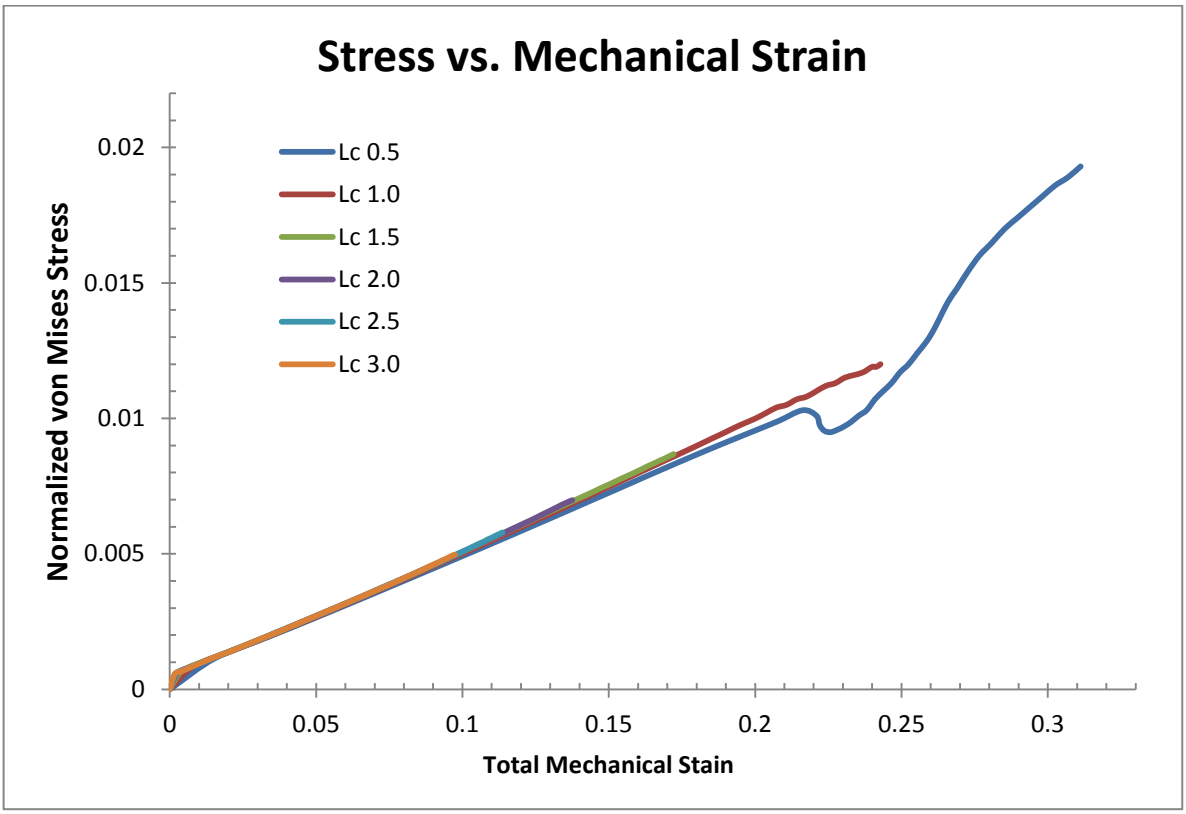

Figure 4.7 Stress-strain Relation

In the corner, the material is pure copper which would not react with lithium, so all the material properties keep the same, not like the silicon and grading part. From Fig 4.6 and 4.7, longer grading length cases has lower stresses. In Fig 4.7, the cases of Lc length from 1.5 to 3.0 shows, the plots are bilinear, and the turning points are all at 0.0006 which is confirm with the assigned copper material properties. So the material yield at stress equals to 0.0006 which is under expectation. For the case of Lc equals to 0.5, the plot has a sharp turning point at 30% Li-ion concentration and shows nonlinear after. In the meantime, nonlinear performance of Lc 0.5 appears after strain of 0.22 which showed in figure 4.7. The reason is that the grading length in this set is short and there is not enough buffering zone. The large deformation on upper silicon rod causes the two adjacent surfaces at the corner contact and squeeze with each other which can be seen in Fig.4.8. That is also the reason for the case of Lc=1.0 got nonlinear

performance after the 39th time step. This contact problem in the corner is an interesting topic for the future study.

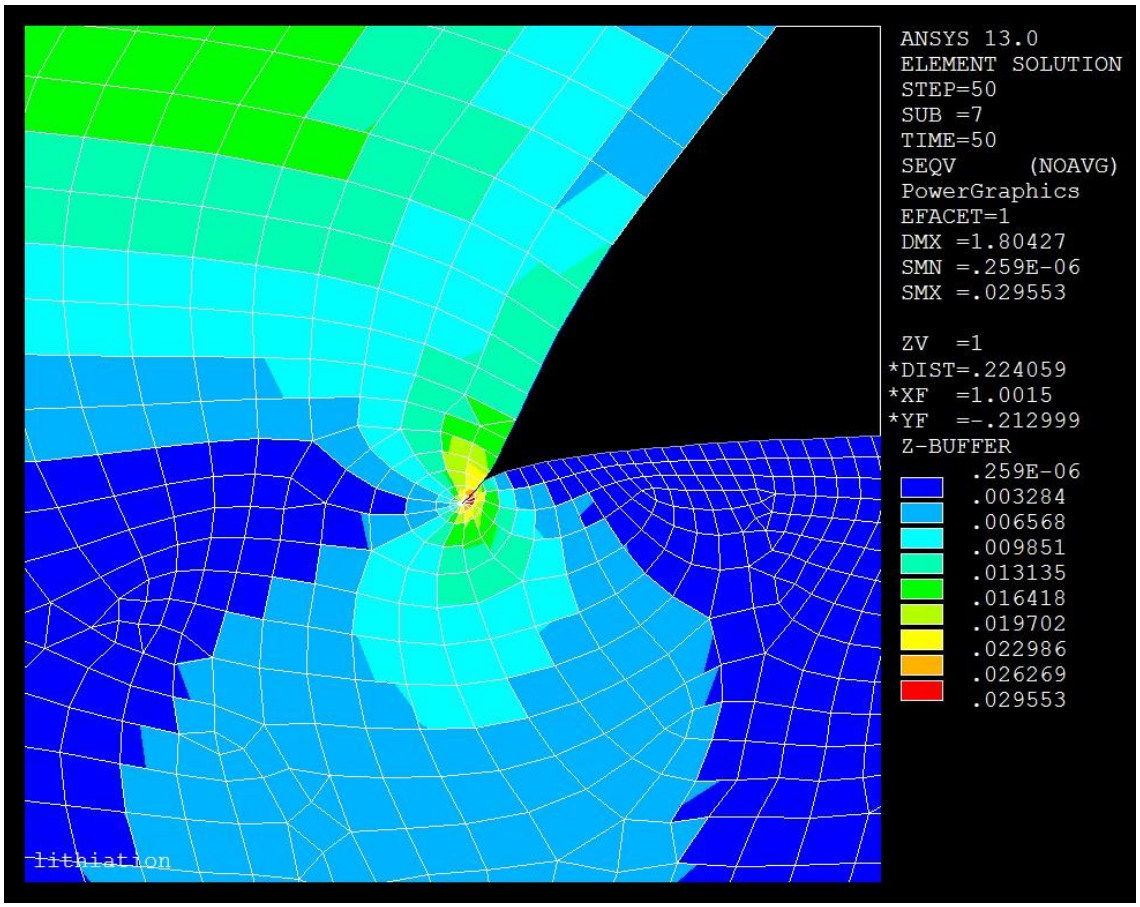

Figure 4.8 Elements contact in Lc=0.5

4.2.3 Comparison of the predicted capacities

In the nanorod structure, only silicon is the active material and reacts with Lithium ions. So the electric capacity of anode is mainly depends on the content of silicon in the nanorods. The capacity for the nanorod of Lc=0.5 is normalized as 1C. Thus, the chart of comparison of the predicted capacities can be seen in Fig.4.7.

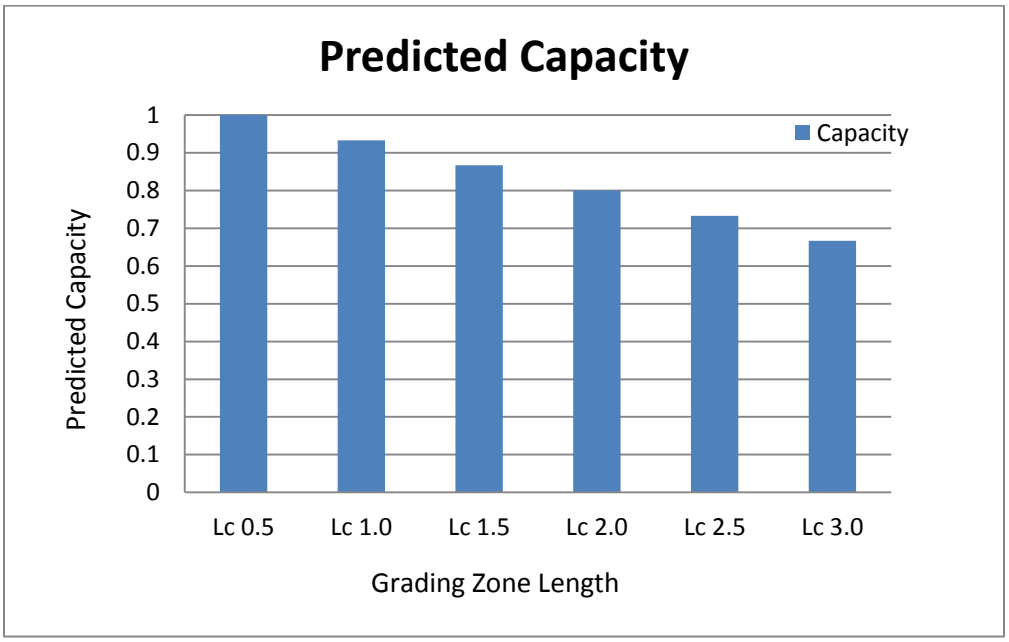

Figure 4.7 Predicted electronic capacities of different cases

The figure above shows that the when the length of the grading zone increases, the capacities decreases. The reason is that the nanorod with longer grading zone has less content of silicon. The case of Lc=3.0 has the capacity of 0.67C which is 33% less than the case of Lc=0.5. So far, the capacity is predicted only base on the contents of the silicon. Experiment values need to support our prediction.

CHAPTER 5

CONCLUSIONS

The results of the FEM simulation show that the stress concentrations locate on the surface of material transition part and the corner between the substrate and rod, which could generate cracks in those locations during the actual charging process. Then the six models of different grading length reveal that the nanorods with longer grading length has lower induced stresses on the surface and corner of the rods. When there is no grading part or the grading length is short, the huge stresses induce by the large swelling in the pure silicon rod would easily cause the large stress concentration in the corner location. With long grading length, the grading zone can release and buffer the stress concentration in the nanorods. Therefore, using composition-graded structure is an effective method to enhance the mechanical reliabilities on the silicon nanorod based lithium-ion battery anode. On the other hand, nanorods with longer grading zone has less electronic capacities. So people need to find the balance between the reliability and the battery capacity based on what they want.

For future works, the grading zone could be design by non-linear material concentrations instead of linear changes to better reduce the stress concentration. On the other hand, the nanorod could be modeled by helix or spring shapes. When swelling occurs during the charging process, the stresses induced are mainly shear stress to the model which is harder to break the materials compared to other types of stresses.

APPENDIX A

ANSYS CODE FOR THE SIMULATION

```
FINISH
/CLEAR
/filename,nanowire_graded
/title,lithiation
/PREP7

!!!!!!! GEOMETRY !!!!!!!!!!!!!!!!

R=1             ! radius of rod
Rcu=2           ! radius of substrate
L=4             ! length of whole nanowire
Lc=1            ! length of CuSi grading zone
Lcr=0.2         ! lenght of pure Cu layer
Lcu=0.5         ! length of pure Cu substrate

NR_elem=30    ! number of elements per radius
NL_elem=NR_elem*L/R  !number of elements per length
NRcu_elem=NR_elem*Rcu/R   !number of elements of cu substrate


!!!!!!! ANALYSIS INPUTS !!!!!!!!!!!!!!

Ts=1            ! maximum temperature (saturation concentration)
TSTEPS=50     ! number of steady state solutions

! material parameters

Si_ex=1                 ! normalized elasticity modulus (young's modulus)
Si_alfa=0.40546         ! coef of thermal expansion
Si_prxy=0.3     ! poisson
Si_yield=0.03   ! yield strength
Si_H=0.1        ! hardening ratio

Cu_ex=0.8       ! elasticity modulus
Cu_alfa=1e-37  ! coef of thermal expansion
Cu_prxy=0.3    ! poisson
Cu_yield=0.0006         ! yield strength
Cu_H=0.05       ! hardening ratio

Li_ex=0.05      !!elasticity modulus of Li
Li_yield=0.0001 !!yield strength

!!!!! 1 silicon atom capture 4.4 Li-ion !!!!!!!!!!!!

SiLi_ex=0.22575         !!SiLi_ex=0.185*1+0.815*0.05=0.22575(full concentration)
SiLi_alfa=0.40546 !! coef of thermal expansion
SiLi_prxy=0.3   !!poisson
SiLi_yield=0.03
SiLi_H=0.05     !!! hardening ratio

!!!!!!!!!!!!!!!!!!!!!!!!!!!!!!!!!!!
!ELEMENT and MATERIAL FORMULATION!
```

```
!!!!!!!!!!!!!!!!!!!!!!!!!!!!!!!!!!

ET,1,PLANE182                    ! element type
KEYOPT,1,3,1            ! axisymetry (y-axis default)
KEYOPT,1,1,0            ! Full integration with B-bar method
KEYOPT,1,6,1            ! mixed u-P formulation

dy=L/NL_elem
N=(Lc)/dy


!! Assigning material properties for the Cu-Si grading

!!!!!!!!!!!!Before lithiation!!!!!!!!!!!!!!!!!!
dCuSiex=(Si_ex-Cu_ex)/N
dCuSialfa=(Si_alfa-Cu_alfa)/N
dCuSiyield=(Si_yield-Cu_yield)/N
dCuSiH=(Si_H-Cu_H)/N
dCuSiprxy=(Si_prxy-Cu_prxy)/N

!!!!!!!!!!!!After lithiation!!!!!!!!!!!!!!!!!!!!
dCuSiLiex=(SiLi_ex-Cu_ex)/N
dCuSiLialfa=(SiLi_alfa-Cu_alfa)/N
dCuSiLiyield=(SiLi_yield-Cu_yield)/N
dCuSiLiH=(SiLi_H-Cu_H)/N
dCuSiLiprxy=(SiLi_prxy-Cu_prxy)/N

A=N         ! number of CuSi part

!! Assigning material property for lithiated Si

!!!!!!! substrate and pure Cu within rod !!!!!!!!


k,1,0,0
k,2,R,0
k,3,R,-Lcr          ! spider mesh keypoint
k,4,Rcu,-Lcr
k,5,Rcu,-Lcr-Lcu
k,6,0,-Lcr-Lcu

a,1,2,3,4,5,6,1

! material pure Cu
MPTEMP,,,,,,,,
MPTEMP,1,0
MPTEMP,2,1              ! two temperature
MPDATA,EX,1,,Cu_ex  ! defined young's modulus(temp dependent material)
MPDATA,EX,1,,Cu_ex
MPDATA,ALPX,1,,Cu_alfa        ! defined thermal conductivity
MPDATA,ALPX,1,,Cu_alfa
MPDATA,PRXY,1,,Cu_prxy       ! defined poisson
```

```
MPDATA,PRXY,1,,Cu_prxy
TB,BISO,1,2
TBTEMP,0
TBDATA,1,Cu_yield,Cu_H
TBTEMP,1
TBDATA,1,Cu_yield,Cu_H

! element size is dy, thus everything will be parametric
! connected with the size so that it works when changing NR_elem


!!!!!!!!!!!!!!!!!!!!!!!!!!!!!!!!!!!!!!!!!!!!!!!!!!!!!!!!!!!!!!!!!!!!!!!
KSCON,3,dy/5,1,15,1              ! spider mesh
!!!!!!!!!!!!!!!!!!!!!!!!!!!!!!!!!!!!!!!!!!!!!!!!!!!!!!!!!!!!!!!!!!!!!!!

AESIZE,1,dy
MSHAPE,0,2D
MSHKEY,0
AMESH,1


!!!!!! grading and pure Si !!!!!!!

! material 2 is pure Si

MPTEMP,,,,,,,,
MPTEMP,1,0
MPTEMP,2,1              ! two temperature(look concentration as temp)
MPDATA,EX,2,,Si_ex    ! defined elasticity modulus
MPDATA,EX,2,,SiLi_ex
MPDATA,ALPX,2,,Si_alfa          ! defined coef of thermal expansion
MPDATA,ALPX,2,,SiLi_alfa
MPDATA,PRXY,2,,Si_prxy        ! defined poisson
MPDATA,PRXY,2,,SiLi_prxy

TB,BISO,2,2
TBTEMP,0
TBDATA,1,Si_yield,Si_H
TBTEMP,1
TBDATA,1,SiLi_yield,SiLi_H

*do,i,0,NL_elem,1


!!!!!!!!!!pure Si!!!!!!!!!!!!!!!!!!

  *IF,i,GE,A,then

    RECTNG,0,R,(i+1)*dy-dy,(i+1)*dy    ! starting from 0 y
    lsel,s,,,6+4*(i+1)-3
    lesize,all,,,NR_elem
    alls
```

```
    lsel,s,,,6+4*(i+1)-1
    lesize,all,,,NR_elem
    alls

    lsel,s,,,6+4*(i+1)-2
    lsel,a,,,6+4*(i+1)
    lesize,all,,,1
    alls

    mat,2
    MSHAPE,0,2D
    MSHKEY,1
    amesh,i+2

!!!!!!!!!!!!!!!!!!!!CuSi grading!!!!!!!!!!!!!!!!!!!!!!

    *else

        RECTNG,0,R,(i+1)*dy-dy,(i+1)*dy

        Cu_Si_ex=Cu_ex+(i+1)*(dCuSiex)
        Cu_Si_alfa=Cu_alfa+(i+1)*(dCuSialfa)
        Cu_Si_yield=Cu_yield+(i+1)*(dCuSiyield)
        Cu_Si_H=Cu_H+(i+1)*(dCuSiH)
        Cu_Si_prxy=Cu_prxy+(i+1)*(dCuSiprxy)

        !!!!!!!!!lithium comes in property!!!!!!!!
        Cu_Si_Li_ex=Cu_ex+(i+1)*(dCuSiLiex)
        Cu_Si_Li_alfa=Cu_alfa+(i+1)*(dCuSiLialfa)
        Cu_Si_Li_yield=Cu_yield+(i+1)*(dCuSiLiyield)
        Cu_Si_Li_H=Cu_H+(i+1)*(dCuSiLiH)
        Cu_Si_Li_prxy=Cu_prxy+(i+1)*(dCuSiLiprxy)

        !thermal prop!
        MPTEMP,,,,,,,,
        MPTEMP,1,0
        MPTEMP,2,1

        !stress prop!
        MPDATA,EX,i+3,,Cu_Si_ex              ! defined density
        MPDATA,EX,i+3,,Cu_Si_Li_ex
        MPDATA,ALPX,i+3,,Cu_Si_alfa          ! defined thermal conductivity
        MPDATA,ALPX,i+3,,Cu_Si_Li_alfa
        MPDATA,PRXY,i+3,,Cu_Si_prxy          ! defined poisson
        MPDATA,PRXY,i+3,,Cu_Si_Li_prxy
        TB,BISO,i+3,2
        TBTEMP,0
        TBDATA,1,Cu_Si_yield,Cu_Si_H
        TBTEMP,1
        TBDATA,1,Cu_Si_Li_yield,Cu_Si_Li_H
```

```
        lsel,s,,,6+4*(i+1)-3
        lesize,all,,,NR_elem
        alls
        lsel,s,,,6+4*(i+1)-1
        lesize,all,,,NR_elem
        alls

        lsel,s,,,6+4*(i+1)-2
        lsel,a,,,6+4*(i+1)
        lesize,all,,,1
        alls

        mat,i+3
        MSHAPE,0,2D
        MSHKEY,1
        amesh,i+2

    *endif
*enddo


nummrg,node


alls

!!!!!!!!!!!!!!!!! STRUCTURAL CONTACTS!!!!!!!!!!!!!!!!!!

ET,2,169        ! target element or contact
ET,3,172        ! contact element or target
TYPE,3          ! element type
MAT,1           ! material
REAL,4
lsel,s,,,3
nsll,s,1
esurf
TYPE,2
lsel,s,,,2
nsll,s,1
esurf
ALLSEL,ALL
!contact
MP,MU,4,        ! contact definition
alls


!!!!!!!!!!!!!!!!!!!!!!!!!!!!!!!!!!!!!!!!!!!!!!!!!!!!!!!
!!!!!!!!!!! APPLY BOUNDARY CONDITIONS !!!!!!!!!!
!!!!!!!!!!!!!!!!!!!!!!!!!!!!!!!!!!!!!!!!!!!!!!!!!!!!!!!

FINISH
/SOL
```

```
PSTRES,ON                       ! Calculate prestress effect

deltaLOC=L/NL_elem

n=1

*do,j,0,Ts,Ts/TSTEPS
   BF,all,TEMP,j                ! assign temperature on selected nodes as TT
   alls                    ! select all
   lsel,s,,,5
   NSLL,S,1                     ! select node 1
   !D,all,UX,0
   D,all,UY,0                   ! fix deformation in Y, otherwise we have free body/rigid body
motion
   alls

   lswrite,n                    ! writte Boundary condition settin ginto file for particular time
step
   n=n+1                              ! assign next time step

*enddo

alls


!!!!!!!!!!!!!!!!!!!!!!!!!!!!!!!!!!
!!!!!!!SOLUTION
!!!!!!!!!!!!!!!!!!!!!!!!!!!!!!!!!!

antype,0                ! steady state
nlgeom,on               ! geometrical nonlinearity
lnsrch,on
LSSOLVE,1,TSTEPS,1,     ! solve timesteps  1 to TSTEPS

FINISH

/post1
set,last
PLESOL, S,EQV, 0,1.0


!!!!!!!!!!!!!!!!!!!!!!!!!!!!!!!
!!!!!!Timehistory plot!!!!!!!
!!!!!!!!!!!!!!!!!!!!!!!!!!!!!!!

/post26
nnodepl=32                      ! corner node is NR_elem+2
ANSOL,2,nnodepl,S,EQV,SEQV_2
STORE,MERGE
XVAR,1
PLVAR,2
```

APPENDIX B

VALUES FOR FIGURE 4.4 & 4.5

%Li	Lc 0.5 ε	Lc 0.5σ	Lc 1.0	Lc 1.0σ	Lc 1.5 ε	Lc 1.5σ	Lc 2.0 ε	Lc 2.0σ	Lc 2.5 ε	Lc 2.5σ	Lc 3.0 ε	Lc 3.0σ
0	0	0	0	0	0	0	0	0	0	0	0	0
1.663	0.0037	3.61E-03	0.00242	2.37E-03	0.00169	1.65E-03	0.00127	1.24E-03	0.00102	9.95E-04	0.000837	8.18E-04
3.326	0.00739	7.08E-03	0.00486	4.68E-03	0.00337	3.23E-03	0.00254	2.44E-03	0.00203	1.96E-03	0.00167	1.61E-03
4.989	0.011	1.04E-02	0.0073	6.91E-03	0.00505	4.77E-03	0.00381	3.60E-03	0.00305	2.88E-03	0.0025	2.37E-03
6.652	0.01444	1.34E-02	0.00973	9.07E-03	0.00673	6.26E-03	0.00507	4.72E-03	0.00406	3.78E-03	0.00334	3.11E-03
8.315	0.01778	1.62E-02	0.01216	1.11E-02	0.0084	7.69E-03	0.00633	5.80E-03	0.00507	4.64E-03	0.00417	3.82E-03
9.978	0.021	1.88E-02	0.01458	1.31E-02	0.0101	9.07E-03	0.0076	6.84E-03	0.00608	5.48E-03	0.005	4.51E-03
11.641	0.024	2.12E-02	0.01698	1.50E-02	0.0118	1.04E-02	0.00886	7.84E-03	0.0071	6.28E-03	0.00583	5.16E-03
13.304	0.027	2.34E-02	0.01938	1.69E-02	0.0134	1.17E-02	0.0101	8.80E-03	0.00811	7.05E-03	0.00666	5.80E-03
14.967	0.02991	2.48E-02	0.02176	1.86E-02	0.0151	1.29E-02	0.0114	9.72E-03	0.00911	7.79E-03	0.00749	6.40E-03
16.63	0.03203	2.57E-02	0.02413	2.03E-02	0.0168	1.41E-02	0.0126	1.06E-02	0.0101	8.50E-03	0.00832	6.98E-03
18.293	0.03425	2.49E-02	0.02648	2.18E-02	0.0184	1.52E-02	0.0139	1.14E-02	0.0111	9.17E-03	0.00915	7.54E-03
19.956	0.03749	2.47E-02	0.0288	2.33E-02	0.0201	1.63E-02	0.0152	1.23E-02	0.0121	9.82E-03	0.00997	8.07E-03
21.619	0.041	2.46E-02	0.03068	2.39E-02	0.0218	1.73E-02	0.0164	1.30E-02	0.0131	1.04E-02	0.0108	8.57E-03
23.282	0.04443	2.44E-02	0.03255	2.34E-02	0.0234	1.82E-02	0.0177	1.37E-02	0.0142	1.10E-02	0.0116	9.05E-03
24.945	0.04777	2.42E-02	0.03539	2.31E-02	0.0251	1.92E-02	0.0189	1.44E-02	0.0152	1.16E-02	0.0125	9.50E-03
26.608	0.05109	2.39E-02	0.03839	2.29E-02	0.0268	2.00E-02	0.0202	1.51E-02	0.0162	1.21E-02	0.0133	9.92E-03
28.271	0.05442	2.37E-02	0.04129	2.27E-02	0.0284	2.08E-02	0.0214	1.57E-02	0.0172	1.26E-02	0.0141	1.03E-02
29.934	0.05774	2.35E-02	0.04417	2.24E-02	0.029361	2.08E-02	0.0227	1.63E-02	0.0182	1.30E-02	0.0149	1.07E-02
31.597	0.06106	2.32E-02	0.04697	2.21E-02	0.03093	2.06E-02	0.0239	1.68E-02	0.0192	1.35E-02	0.0158	1.10E-02
33.26	0.06437	2.29E-02	0.04974	2.19E-02	0.03306	2.03E-02	0.0252	1.73E-02	0.0202	1.39E-02	0.0166	1.14E-02
34.923	0.06769	2.27E-02	0.05241	2.16E-02	0.03553	2.00E-02	0.0265	1.78E-02	0.0212	1.42E-02	0.0174	1.17E-02
36.586	0.07002	2.24E-02	0.05502	2.13E-02	0.03791	1.97E-02	0.0277	1.82E-02	0.0222	1.46E-02	0.0182	1.19E-02
38.249	0.07335	2.21E-02	0.0576	2.10E-02	0.0404	1.94E-02	0.029	1.86E-02	0.0232	1.49E-02	0.019	1.22E-02
39.9	0.07	2.19	0.06	2.06	0.04	1.91	0.02	1.79	0.02	1.51	0.01	1.24

12	69	E-02	011	E-02	28	E-02	912	E-02	42	E-02	99	E-02
41.575	0.0805	2.16E-02	0.06259	2.03E-02	0.0453	1.88E-02	0.0307	1.78E-02	0.0252	1.54E-02	0.0207	1.26E-02
43.238	0.0842	2.14E-02	0.065	2.00E-02	0.0476	1.85E-02	0.03228	1.74E-02	0.0262	1.56E-02	0.0215	1.28E-02
44.901	0.088	2.11E-02	0.06738	1.96E-02	0.0501	1.82E-02	0.0341	1.71E-02	0.0272	1.58E-02	0.0223	1.29E-02
46.564	0.0918	2.08E-02	0.06974	1.93E-02	0.0525	1.79E-02	0.03595	1.67E-02	0.0282	1.59E-02	0.0232	1.30E-02
48.227	0.0958	2.06E-02	0.07205	1.89E-02	0.0547	1.75E-02	0.03785	1.64E-02	0.028517	1.55E-02	0.024	1.31E-02
49.89	0.0997	2.03E-02	0.07434	1.86E-02	0.0569	1.72E-02	0.03963	1.60E-02	0.029262	1.52E-02	0.0248	1.32E-02
51.553	0.1037	2.00E-02	0.07662	1.82E-02	0.059	1.68E-02	0.0415	1.57E-02	0.03048	1.49E-02	0.0256	1.32E-02
53.216	0.1078	1.97E-02	0.07887	1.78E-02	0.0611	1.65E-02	0.0434	1.53E-02	0.0318	1.45E-02	0.0265	1.33E-02
54.879	0.1118	1.95E-02	0.08109	1.74E-02	0.0631	1.61E-02	0.0453	1.49E-02	0.03331	1.41E-02	0.0273	1.33E-02
56.542	0.1158	1.92E-02	0.0833	1.70E-02	0.0651	1.57E-02	0.0471	1.46E-02	0.03477	1.38E-02	0.0276	1.30E-02
58.205	0.1198	1.88E-02	0.08553	1.66E-02	0.0671	1.53E-02	0.0489	1.42E-02	0.03624	1.34E-02	0.028459	1.29E-02
59.868	0.1237	1.85E-02	0.08778	1.63E-02	0.0689	1.49E-02	0.0507	1.38E-02	0.03772	1.30E-02	0.029391	1.26E-02
61.531	0.1277	1.82E-02	0.09005	1.59E-02	0.0707	1.45E-02	0.0526	1.34E-02	0.03928	1.26E-02	0.0297	1.20E-02
63.194	0.1316	1.79E-02	0.09233	1.55E-02	0.0724	1.41E-02	0.0544	1.30E-02	0.0407	1.22E-02	0.03076	1.16E-02
64.857	0.1355	1.75E-02	0.09443	1.50E-02	0.0741	1.37E-02	0.0561	1.27E-02	0.0423	1.18E-02	0.0319	1.12E-02
66.52	0.1395	1.72E-02	0.09681	1.46E-02	0.0758	1.33E-02	0.0578	1.23E-02	0.0437	1.14E-02	0.03309	1.08E-02
68.183	0.1433	1.68E-02	0.09927	1.42E-02	0.0775	1.29E-02	0.0595	1.18E-02	0.0452	1.10E-02	0.03416	1.04E-02
69.846	0.1471	1.64E-02	0.10164	1.38E-02	0.0791	1.24E-02	0.0612	1.14E-02	0.0466	1.06E-02	0.03542	9.99E-03
71.509	0.150865	1.61E-02	0.10416	1.34E-02	0.0807	1.20E-02	0.0628	1.10E-02	0.0481	1.02E-02	0.03668	9.57E-03
73.172	0.154722	1.56E-02	0.10657	1.29E-02	0.0823	1.15E-02	0.0644	1.06E-02	0.0496	9.77E-03	0.0379	9.14E-03
74.835	0.158598	1.52E-02	0.10902	1.25E-02	0.0837	1.11E-02	0.0659	1.01E-02	0.051	9.33E-03	0.0392	8.71E-03
76.498	0.162477	1.48E-02	0.1114	1.20E-02	0.0852	1.06E-02	0.0673	9.67E-03	0.0524	8.89E-03	0.0404	8.27E-03
78.161	0.166246	1.43E-02	0.11375	1.15E-02	0.0866	1.01E-02	0.0687	9.20E-03	0.0538	8.45E-03	0.0416	7.83E-03
79.824	0.169964	1.38E-02	0.11601	1.11E-02	0.088	9.62E-03	0.07	8.73E-03	0.0552	8.00E-03	0.0428	7.39E-03
81.4	0.17	1.33	0.11	1.06	0.08	9.14	0.07	8.25	0.05	7.55	0.04	6.94

87	3606	E-02	825	E-02	94	E-03	12	E-03	64	E-03	4	E-03

APPENDIX C

VALUES FOR FIGURE 4.6 & 4.7

%Li	Lc 0.5 ε	Lc 0.5σ	Lc 1.0 ε	Lc 1.0σ	Lc 1.5 ε	Lc 1.5σ	Lc 2.0 ε	Lc 2.0σ	Lc 2.5 ε	Lc 2.5σ	Lc 3.0 ε	Lc 3.0σ
0	0	0	0	0	0	0	0	0	0	0	0	0
1.663	0.01547	1.15E-03	0.008057	8.45E-04	4.16E-03	6.74E-04	2.72E-03	6.09E-04	2.07E-03	5.79E-04	1.69E-03	5.61E-04
3.326	0.03361	1.93E-03	0.020697	1.39E-03	1.29E-02	1.08E-03	8.23E-03	8.60E-04	5.52E-03	7.38E-04	4.04E-03	6.70E-04
4.989	0.04865	2.59E-03	0.030087	1.79E-03	2.05E-02	1.39E-03	1.47E-02	1.16E-03	1.09E-02	9.86E-04	8.02E-03	8.51E-04
6.652	0.06252	3.21E-03	0.038519	2.17E-03	2.67E-02	1.66E-03	2.02E-02	1.38E-03	1.57E-02	1.20E-03	1.25E-02	1.06E-03
8.315	0.07554	3.80E-03	0.046517	2.52E-03	3.24E-02	1.91E-03	2.49E-02	1.58E-03	2.00E-02	1.38E-03	1.63E-02	1.23E-03
9.978	0.08803	4.37E-03	0.053989	2.86E-03	3.77E-02	2.15E-03	2.91E-02	1.77E-03	2.37E-02	1.54E-03	1.99E-02	1.37E-03
11.641	0.10008	4.92E-03	0.061345	3.20E-03	4.28E-02	2.38E-03	3.32E-02	1.95E-03	2.72E-02	1.69E-03	2.29E-02	1.50E-03
13.304	0.11157	5.45E-03	0.068389	3.52E-03	4.76E-02	2.60E-03	3.70E-02	2.12E-03	3.04E-02	1.83E-03	2.58E-02	1.63E-03
14.967	0.122703	5.97E-03	0.075221	3.84E-03	5.24E-02	2.81E-03	4.08E-02	2.29E-03	3.36E-02	1.97E-03	2.86E-02	1.75E-03
16.63	0.133395	6.47E-03	0.081942	4.15E-03	5.69E-02	3.02E-03	4.43E-02	2.45E-03	3.66E-02	2.11E-03	3.13E-02	1.87E-03
18.293	0.143752	6.96E-03	0.088454	4.46E-03	6.14E-02	3.23E-03	4.78E-02	2.61E-03	3.96E-02	2.24E-03	3.39E-02	1.98E-03
19.956	0.153736	7.43E-03	0.094755	4.76E-03	6.58E-02	3.43E-03	5.12E-02	2.77E-03	4.25E-02	2.37E-03	3.64E-02	2.09E-03
21.619	0.163392	7.89E-03	0.100943	5.05E-03	7.01E-02	3.63E-03	5.46E-02	2.92E-03	4.52E-02	2.49E-03	3.88E-02	2.20E-03
23.282	0.172776	8.33E-03	0.106918	5.34E-03	7.44E-02	3.83E-03	5.79E-02	3.07E-03	4.80E-02	2.62E-03	4.12E-02	2.31E-03
24.945	0.181919	8.75E-03	0.112603	5.62E-03	7.86E-02	4.03E-03	6.11E-02	3.22E-03	5.07E-02	2.74E-03	4.35E-02	2.41E-03
26.608	0.190827	9.15E-03	0.11814	5.89E-03	8.27E-02	4.22E-03	6.43E-02	3.37E-03	5.34E-02	2.86E-03	4.58E-02	2.52E-03
28.271	0.199516	9.53E-03	0.123499	6.16E-03	8.67E-02	4.42E-03	6.74E-02	3.51E-03	5.59E-02	2.98E-03	4.80E-02	2.62E-03
29.934	0.207919	9.90E-03	0.128693	6.41E-03	9.07E-02	4.61E-03	7.05E-02	3.66E-03	5.85E-02	3.10E-03	5.03E-02	2.72E-03
31.597	0.216234	1.03E-02	0.133729	6.66E-03	9.47E-02	4.80E-03	7.35E-02	3.80E-03	6.09E-02	3.21E-03	5.24E-02	2.82E-03
33.26	0.220948	1.01E-02	0.138614	6.91E-03	9.85E-02	4.99E-03	7.66E-02	3.94E-03	6.35E-02	3.33E-03	5.46E-02	2.92E-03
34.923	0.222111	9.74E-03	0.143362	7.14E-03	1.02E-01	5.18E-03	7.95E-02	4.08E-03	6.59E-02	3.44E-03	5.67E-02	3.01E-03
36.5	0.223	9.54	0.147	7.38	1.06	5.36	8.25	4.22	6.83	3.55	5.88	3.11

86	679	E-03	981	E-03	E-01	E-03	E-02	E-03	E-02	E-03	E-02	E-03
38.249	0.225723	9.49E-03	0.152477	7.60E-03	1.10E-01	5.54E-03	8.54E-02	4.36E-03	7.07E-02	3.67E-03	6.08E-02	3.20E-03
39.912	0.227916	9.57E-03	0.156869	7.82E-03	1.13E-01	5.72E-03	8.82E-02	4.50E-03	7.31E-02	3.78E-03	6.28E-02	3.30E-03
41.575	0.230366	9.70E-03	0.161163	8.04E-03	1.17E-01	5.89E-03	9.11E-02	4.64E-03	7.54E-02	3.89E-03	6.49E-02	3.39E-03
43.238	0.232817	9.87E-03	0.165371	8.25E-03	1.20E-01	6.05E-03	9.39E-02	4.77E-03	7.77E-02	3.99E-03	6.68E-02	3.48E-03
44.901	0.235386	1.01E-02	0.1695	8.46E-03	1.23E-01	6.21E-03	9.66E-02	4.90E-03	8.00E-02	4.10E-03	6.87E-02	3.57E-03
46.564	0.238099	1.03E-02	0.173555	8.66E-03	1.26E-01	6.37E-03	9.93E-02	5.04E-03	8.22E-02	4.21E-03	7.06E-02	3.66E-03
48.227	0.240909	1.07E-02	0.177533	8.86E-03	1.29E-01	6.52E-03	1.02E-01	5.17E-03	8.44E-02	4.31E-03	7.26E-02	3.75E-03
49.89	0.243681	1.10E-02	0.181452	9.06E-03	1.32E-01	6.66E-03	1.05E-01	5.30E-03	8.65E-02	4.42E-03	7.44E-02	3.83E-03
51.553	0.246584	1.13E-02	0.185303	9.26E-03	1.35E-01	6.80E-03	1.07E-01	5.42E-03	8.87E-02	4.52E-03	7.62E-02	3.92E-03
53.216	0.249512	1.17E-02	0.189098	9.45E-03	1.37E-01	6.93E-03	1.10E-01	5.55E-03	9.07E-02	4.62E-03	7.79E-02	4.00E-03
54.879	0.252457	1.20E-02	0.192847	9.65E-03	1.40E-01	7.06E-03	1.12E-01	5.67E-03	9.27E-02	4.72E-03	7.96E-02	4.09E-03
56.542	0.255329	1.24E-02	0.196541	9.83E-03	1.42E-01	7.18E-03	1.14E-01	5.78E-03	9.47E-02	4.81E-03	8.13E-02	4.17E-03
58.205	0.258308	1.28E-02	0.200178	1.00E-02	1.45E-01	7.30E-03	1.17E-01	5.90E-03	9.66E-02	4.91E-03	8.29E-02	4.24E-03
59.868	0.260663	1.32E-02	0.20376	1.02E-02	1.47E-01	7.42E-03	1.19E-01	6.01E-03	9.84E-02	5.00E-03	8.44E-02	4.32E-03
61.531	0.263061	1.37E-02	0.207293	1.04E-02	1.49E-01	7.53E-03	1.21E-01	6.12E-03	1.00E-01	5.09E-03	8.59E-02	4.39E-03
63.194	0.265882	1.43E-02	0.21077	1.05E-02	1.52E-01	7.64E-03	1.23E-01	6.22E-03	1.02E-01	5.17E-03	8.73E-02	4.46E-03
64.857	0.269004	1.48E-02	0.214186	1.07E-02	1.54E-01	7.75E-03	1.25E-01	6.32E-03	1.03E-01	5.25E-03	8.86E-02	4.53E-03
66.52	0.272557	1.54E-02	0.217544	1.08E-02	1.56E-01	7.85E-03	1.27E-01	6.42E-03	1.05E-01	5.33E-03	8.98E-02	4.59E-03
68.183	0.276562	1.60E-02	0.22085	1.10E-02	1.58E-01	7.95E-03	1.28E-01	6.51E-03	1.06E-01	5.40E-03	9.10E-02	4.65E-03
69.846	0.281046	1.65E-02	0.224178	1.12E-02	1.60E-01	8.05E-03	1.30E-01	6.59E-03	1.07E-01	5.46E-03	9.21E-02	4.70E-03
71.509	0.285278	1.70E-02	0.227375	1.13E-02	1.62E-01	8.15E-03	1.31E-01	6.67E-03	1.09E-01	5.53E-03	9.31E-02	4.76E-03
73.172	0.28961	1.74E-02	0.230595	1.15E-02	1.64E-01	8.25E-03	1.33E-01	6.74E-03	1.10E-01	5.58E-03	9.40E-02	4.80E-03
74.8	0.293	1.78	0.233	1.16	1.65	8.34	1.34	6.81	1.11	5.63	9.48	4.84

35	897	E-02	818	E-02	E-01	E-03	E-01	E-03	E-01	E-03	E-02	E-03
76.498	0.298224	1.82E-02	0.236896	1.17E-02	1.67E-01	8.43E-03	1.35E-01	6.86E-03	1.12E-01	5.68E-03	9.55E-02	4.88E-03
78.161	0.302545	1.86E-02	0.239944	1.19E-02	1.69E-01	8.51E-03	1.36E-01	6.91E-03	1.12E-01	5.72E-03	9.63E-02	4.92E-03
79.824	0.306901	1.89E-02	0.241345	1.19E-02	1.71E-01	8.60E-03	1.37E-01	6.95E-03	1.13E-01	5.76E-03	9.69E-02	4.95E-03
81.487	0.311219	1.93E-02	0.24284	1.20E-02	1.72E-01	8.68E-03	1.38E-01	6.98E-03	1.14E-01	5.79E-03	9.74E-02	4.97E-03

REFERENCES

[1] "What is Lithium Battery," GasTon, [Online]. Available: http://www.gaston-lithium.com/tech-certificates.html. [Accessed 10 2 2013].

[2] J. P. R. Z. Mehul Oswal, "A comparative study of Lithium-ion Batteries," University of Southern California, 2010.

[3] nexeon.co.uk, "Nexeon technology overview," nexeon.co.uk, 2013. [Online]. Available: http://www.nexeon.co.uk/technology/. [Accessed 10 2 2013].

[4] J. T. H. B. A. K. K. J. S. Sankaran Murugesan, "Copper-Coated Amorphous Silicon Particles as an Anode Material for," Chemistry of Materials, pp. 1306-1315, 2012.

[5] A. D. Long Shen, "Research Progress of High Capacity Si Based Anode Material for Li-ion Battery," JOURNAL OF SHANGHAI SECOND POLYTECHNIC UNIVERSITY, vol. 29, no. 3, pp. 191-197, 2012.

[6] S. K. M. Y. Nikolay Dimov, "Carbon-coated silicon as anode material for lithium ion batteries:," Electrochimica Acta, vol. 48, pp. 1579-1587, 2003.

[7] Y. M. L. B.-S. K. J.-S. S. a. J. W. C. Tae Hoon Hwang, "Electrospun Core−Shell Fibers for Robust Silicon Nanoparticle-Based," Nano Letters, vol. 12, pp. 802-807, 2012.

[8] K. K. V. S. Vijay A. Sethuraman, "Increased cycling efficiency and rate capability of copper-coated," Journal of Power Sources, vol. 196, pp. 393-398, 2011.

[9] J. I. Y.-P. H. C. A. L. Y.-P. Z. B. Yang, "A Chemo-Elastoplastic Analysis of Anisotropic Swelling in an SnO2 Nanowire Under Lithiation," Journal of engineering materials and technology, vol. 134, no. 031013-1-031013-5, 2012.

[10] T. B. D. S. S. Bourderau, "Amorphous silicon as a possible anode material for Li-ion batteries," Journal of Power Sources, Vols. 81-82, pp. 233-236, 1999.

[11] J. S. K. T. K. S. T. T. Makiko Uehara a, "Thick vacuum deposited silicon films suitable for the," Journal of Power Sources, vol. 146, pp. 441-444, 2005.

[12] H. Z. C. Y. W. Q. Hong Guo, "A nanosized silicon thin film as high capacity anode," Materials Science and Engineering, vol. 131, pp. 173-176, 2006.

[13] J. C. Kyu Tae Lee, "Roles of nanosize in lithium reactive nanomaterials," Nano Today, vol. 6, pp. 28-41, 2011.

[14] L. Z. H. X. M. T. Z. J. Y. H. Xiao Hua Liu, "Size-Dependent Fracture of Silicon," ASCNANO, vol. 6, no. 2, pp. 1522-1531, 2012.

[15] n. battery, "Disadvantages for organizations to use nanowire battery," 8 2 2009. [Online]. Available: http://jianhualiucomm301.blogspot.com/. [Accessed 10 2 2013].

[16] B. Y. K. Y. C. B. R. R. H. W. C. L. Z. Yuping He, "Designing Si-based nanowall arrays by dynamic shadowing growth to tailor," Journal of Materials Chemistry, vol. 22, pp. 8294-8303, 2012.

[17] J. N. Richard G.Budynas, Shigley's Mechanical Engineering Design, New York: Mc-Graw Hill, 2009.

[18] D. S. M. M. E. P. R. J. Robert D. Cook, "Plasticity: general formulation for small strains," in Concepts and Applications of Finite Element Analysis, Hoboken, John Wiley & Sons. Inc, 2002, pp. 606-612.

[19] Y.-P. H. J. I. ,. C. L. J. R. Y.-P. Z. B. Yanga, "Effects of composition-dependent modulus, finite concentration and boundary," Journal of Power Sources, vol. 204, pp. 168-176, 2012.

BIOGRAPHICAL INFORMATION

Chao Ji started his undergraduate program in 2006 at Shanghai Ocean University, China. In 2008, he participated the joint-degree program and continued his undergraduate program in Florida Institute of Technology. He received his bachelor degrees from both Shanghai Ocean University and Florida Institute of Technology in 2010. After that, he pursued his master degree in University of Texas at Arlington in 2011 and started working under the guidance of Dr. Bo Yang in 2012. His research interests include finite element analysis, stress analysis, structural design, Lithium-ion battery, and computer aided engineering and design.